Neurobiology of Disease

Collagen VI Regulates Motor Circuit Plasticity and Motor Performance by Cannabinoid Modulation

Daniel D. Lam,[1,2] **Rhìannan H. Williams,**[1] **Ernesto Lujan,**[3] **Koji Tanabe,**[3] **Georg Huber,**[4] **Nay Lui Saw,**[5] **Juliane Merl-Pham,**[6] **Aaro V. Salminen,**[1] **David Lohse,**[1] **Sally Spendiff,**[7] **Melanie J. Plastini,**[8] **Michael Zech,**[1,2] **Hanns Lochmüller,**[7,9,10] **Arie Geerlof,**[4] **Stefanie M. Hauck,**[6] **Mehrdad Shamloo,**[5] **Marius Wernig,**[3] **and Juliane Winkelmann**[1,2,11,12]

[1]Institute of Neurogenomics, Helmholtz Zentrum München, Munich, Germany, [2]Institute of Human Genetics, School of Medicine, Technical University of Munich, Munich, Germany, [3]Institute for Stem Cell Biology and Regenerative Medicine, Department of Pathology, Stanford University, Stanford, California 94305, [4]Protein Expression and Purification Facility, Institute of Structural Biology, Helmholtz Zentrum München, Munich, Germany, [5]Department of Neurosurgery, Stanford University School of Medicine, Palo Alto, California 94304, [6]Research Unit Protein Science, Helmholtz Zentrum München, Munich, Germany, [7]Children's Hospital of Eastern Ontario Research Institute, Ottawa, Ontario K1H 5B2, Canada, [8]Department of Neurology and Neurological Sciences, Stanford University School of Medicine, Palo Alto, California 94304, [9]Division of Neurology, Department of Medicine, The Ottawa Hospital, Ottawa, Ontario K1H 8L6, Canada, [10]Brain and Mind Research Institute, University of Ottawa, Ottawa, ON K1N 6N5, Canada, [11]Munich Cluster for Systems Neurology (SyNergy), Munich, Germany, and [12]Lehrstuhl für Neurogenetik, Technische Universität München, Munich, Germany

Collagen VI is a key component of muscle basement membranes, and genetic variants can cause monogenic muscular dystrophies. Conversely, human genetic studies recently implicated collagen VI in central nervous system function, with variants causing the movement disorder dystonia. To elucidate the neurophysiological role of collagen VI, we generated mice with a truncation of the dystonia-related collagen α3 VI (COL6A3) C-terminal domain (CTD). These *Col6a3*[CTT] mice showed a recessive dystonia-like phenotype in both sexes. We found that COL6A3 interacts with the cannabinoid receptor 1 (CB1R) complex in a CTD-dependent manner. *Col6a3*[CTT] mice of both sexes have impaired homeostasis of excitatory input to the basal pontine nuclei (BPN), a motor control hub with dense COL6A3 expression, consistent with deficient endocannabinoid (eCB) signaling. Aberrant synaptic input in the BPN was normalized by a CB1R agonist, and motor performance in *Col6a3*[CTT] mice of both sexes was improved by CB1R agonist treatment. Our findings identify a readily therapeutically addressable synaptic mechanism for motor control.

Key words: basal pontine nuclei; cannabinoid receptor; collagen VI; dystonia; endocannabinoid; synaptic homeostasis

---

Significance Statement

Dystonia is a movement disorder characterized by involuntary movements. We previously identified genetic variants affecting a specific domain of the COL6A3 protein as a cause of dystonia. Here, we created mice lacking the affected domain and observed an analogous movement disorder. Using a protein interaction screen, we found that the affected COL6A3 domain mediates an interaction with the cannabinoid receptor 1 (CB1R). Concordantly, our COL6A3-deficient mice showed a deficit in synaptic plasticity linked to a deficit in cannabinoid signaling. Pharmacological cannabinoid augmentation rescued the motor impairment of the mice. Thus, cannabinoid augmentation could be a promising avenue for treating dystonia, and we have identified a possible molecular mechanism mediating this.
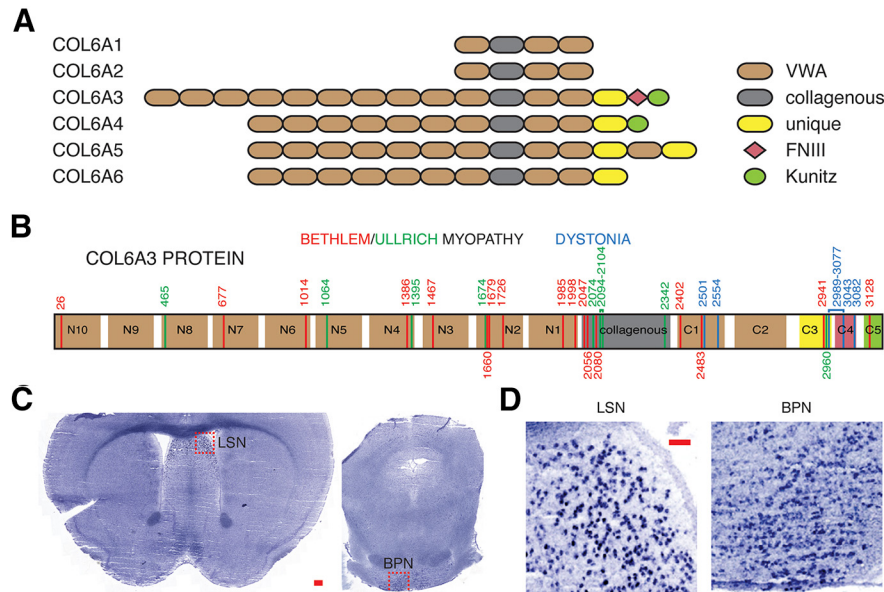

Figure 1. Domains and expression of COL6A3. **A**, Domains of collagen VI subunits. VWA, von Willebrand factor type A; FNIII, fibronectin Type III. **B**, Domains of COL6A3, including globular N-terminal domain (N1–10), collagenous domain, and globular CTD (C1–5). Indicated are amino acid positions of disease-associated variants from UniProt and other reports (Demir et al., 2002; Briñas et al., 2010; Zhang et al., 2014; Marakhonov et al., 2018; Shimomura et al., 2019; UniProt Consortium,2019). **C**, Primary sites of adult mouse brain *Col6a3* expression (dark purple) by *in situ* hybridization in coronal sections. Highlighted are the LSN and BPN, where expression is most concentrated. Scale bar: 200 μm. **D**, Magnification of boxed areas in **C**. Scale bar: 50 μm.

Introduction

Collagen VI forms supramolecular microfibrillary networks in the extracellular matrix (Timpl and Chu, 1994). It is a major component of muscle basement membrane, where it supports muscle stiffness and elasticity structurally as well as by regulating cellular processes (Irwin et al., 2003; Grumati et al., 2010; Urciuolo et al., 2013). Variants in collagen VI-encoding genes can cause monogenic muscular dystrophies because of the integral role of collagen VI in muscle function (Bönnemann, 2011).

Collagen VI is assembled from three subunits, one of which is collagen α3 (VI) or COL6A3 (Timpl and Chu, 1994; Fig. 1A). We recently identified bi-allelic point and indel mutations of the unique COL6A3 C-terminal domain (CTD) in early-onset dystonia (Zech et al., 2015), a movement disorder characterized by sustained or paroxysmal involuntary abnormal movements and/or postures (Albanese et al., 2013). This suggests a CTD-dependent function of COL6A3 in the central nervous system.

To unravel the mechanism linking the COL6A3 CTD with dystonia, we generated *Col6a3*^{CTT} mice with a truncation of this domain and observed a recessive dystonia-like phenotype. Probing the molecular mechanism, we identified a CTD-dependent interaction between COL6A3 and the cannabinoid receptor 1 (CB1R) complex. The endocannabinoid (eCB) system restrains synaptic input and maintains synaptic homeostasis via inhibitory retrograde signaling (Wilson and Nicoll, 2001). In *Col6a3*^{CTT} mice, this process was impaired in neurons of the basal pontine nuclei (BPN), a motor control interface between motor cortex and cerebellum with dense COL6A3 expression. This synaptic deficit, leading to inadequate synaptic downscaling, is a plausible mechanism for hallmarks of dystonia including the central hyperkinetic aspect, impaired surround inhibition, and task-specific manifestations (Quartarone and Pisani, 2011; Calabresi et al., 2016).

Despite these synaptic deficits, CB1R remained intact and could be targeted with an agonist *in vivo*, where this treatment significantly improved motor performance in *Col6a3*^{CTT} mice. Thus, cannabinoid augmentation represents a promising noninvasive therapeutic modality with robust neurophysiological evidence.

Materials and Methods

Experimental model and subject details

A total of 159 mutant or wild-type mice on a C57BL/6 background aged 0–402 d were used in the experiments. Six male wild-type and three male Col6a3$^{CTT/CTT}$ mice were used for *in situ* hybridization studies; 51 wild-type, 16 Col6a3$^{+/CTT}$, and 36 Col6a3$^{CTT/CTT}$ mice (31 male, 72 female) were used for behavioral studies. Six male wild-type and six male Col6a3$^{CTT/CTT}$ mice were used for muscle histology studies. Two male and two female wild-type mice were used to prepare brain lysates for binding partner studies. A total of 15 wild-type and 11 Col6a3$^{CTT/CTT}$ mice (13 male, 13 female) were used for electrophysiology studies. Three male and two female wild-type mice were used to prepare primary cortical neurons. Sample size for behavioral experiments was in accordance with guidelines set by the Stanford Behavioral and Functional Neuroscience Laboratory, which conducted the initial phenotypic analysis. Sample size for electrophysiology was determined based on previously published studies, and statistical significance was calculated using *post hoc* tests. For the crossover study, treatment order was randomized with the randomizr R package, complete_ra function. Experimenters were blinded to animal genotype in all behavioral studies. All animal work was performed in accordance with the German Animal Welfare Act, European Union Directive 2010/63, and the National Institutes of Health *Guide for the Care and Use of Laboratory Animals*, and approved by the Government of Upper Bavaria and the Stanford Administrative Panel on Laboratory Animal Care.

Animals were kept in individually ventilated Tecniplast Greenline GM 500 cages (501-cm² floor area) with laboratory animal bedding (wood fiber/wood chips) and autoclaved nesting material (nestlets, cardboard houses, plastic igloos, or cellulose). Animals were maintained under specified pathogen-free (SPF) conditions in fully air-conditioned rooms with a 12/12 h light/dark cycle, a temperature of 20–24°C and humidity of 45–65%. The cages were changed on average once a week, and animals received sterile filtered water and standard rodent diet *ad libitum*.

Histology

For *in situ* hybridization, animals were euthanized by cervical dislocation. Fresh brains were extracted, snap frozen in −60°C isopentane (2-
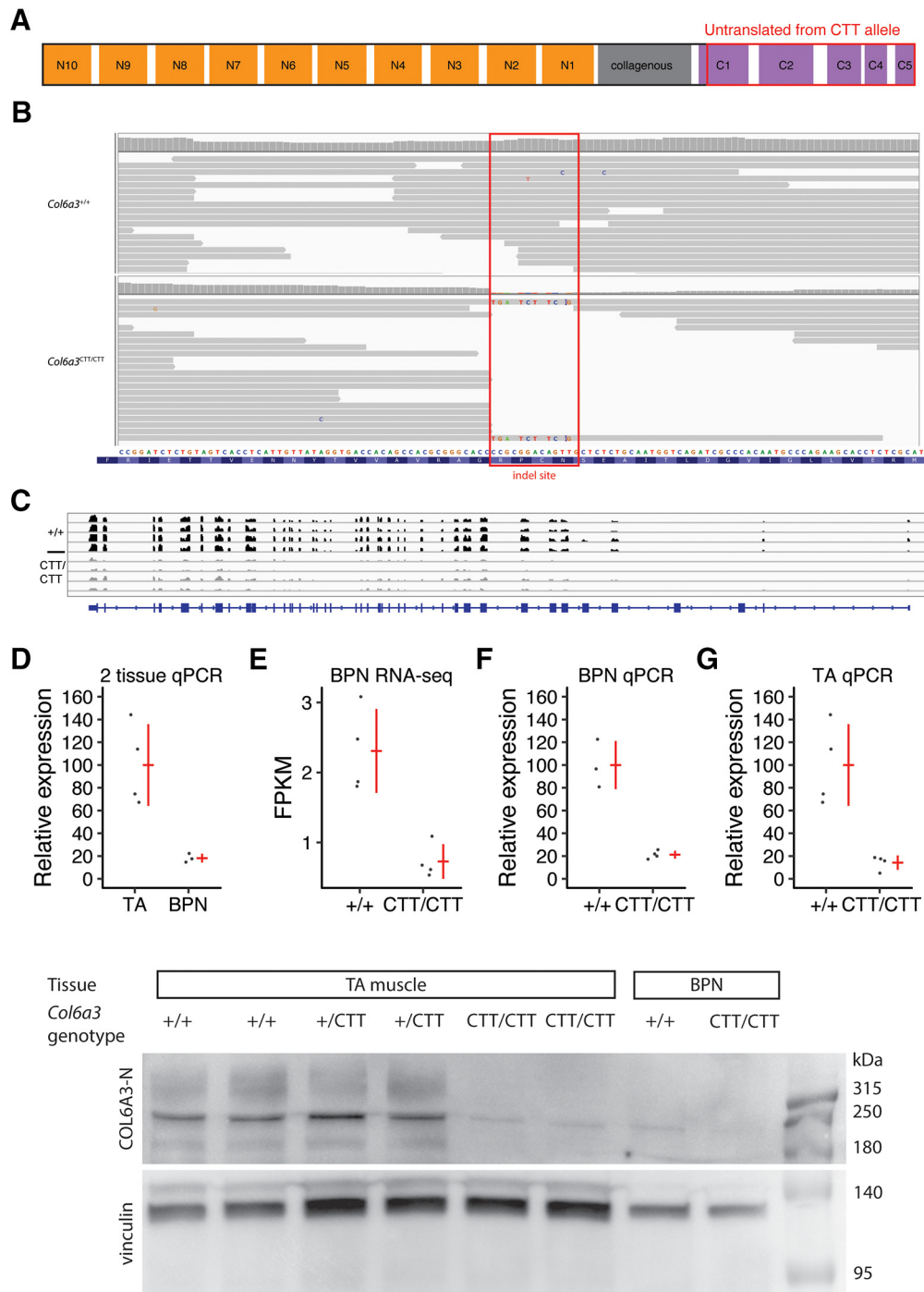
Figure 2. Validation of *Col6a3*^CTT allele. ***A***, Domains of COL6A3, indicating segment which is untranslated from the *Col6a3*^CTT allele. ***B***, Aligned BPN RNA-seq reads verify the CTT mutation at the RNA level. ***C***, BPN RNA-seq read pileups at the *Col6a3* locus, n = 4 replicates per genotype. ***D***, Comparison of BPN and tibialis anterior (TA) muscle expression by qPCR. ***E–G***, Reduced expression in *Col6a3*^CTT/CTT mice in BPN according to RNA-seq (***E***) and qPCR (***F***), and in TA according to qPCR (***G***). ***H***, Western blotting detection of COL6A3 N-terminal domain in TA muscle and BPN.

methylbutane), sectioned at 30-μm thickness on a cryostat, and collected on Superfrost slides. For chromogenic *in situ* hybridization, sections were fixed in 4% paraformaldehyde (PFA) in PBS for 10 min, then rinsed in PBS. After three 10 min PBS washes, sections were acetylated in 1.35% triethanolamine, 0.02 N hydrochloric acid, and 0.25% (v/v) acetic anhydride for 10 min. Next, sections were permeabilized with 1% (v/v) Triton X-100 in PBS, followed by three 10-min PBS washes. Sections were then prehybridized with hybridization solution (50% formamide, 10% dextran sulfate, 2% Denhardt's solution, 1 mg/ml yeast transfer RNA, 300 mM NaCl, 10 mM Tris-HCl pH 6.5, 5 mM EDTA pH 8, 50 mM NaH$_2$PO$_4$, 50 mM Na$_2$HPO$_4$) for 2–4 h.

To synthesize the riboprobe, a 509 bp cDNA fragment spanning the C-terminal encoding portion of the transcript (base 9548–10,056 of Ensembl transcript ENSMUST00000056925.15, spanning exons 40–43) was cloned from mouse brain cDNA into pCRII-TOPO (Thermo Fisher Scientific). The plasmid was linearized and subjected to *in vitro* transcription with digoxigenin labeling (DIG RNA labeling kit, Sigma). Sections were hybridized with 500 ng/ml riboprobe in hybridization solution at 72°C overnight. Next, sections were incubated with 0.2× saline sodium citrate (SSC; 30 mM NaCl, 3 mM trisodium citrate, pH 7) at 72°C for 45 min, then washed in 0.2× SSC for 5 min. To detect digoxigenin, sections were blocked in B1 (100 mM Tris-HCl pH 7.5, 150 mM NaCl, 0.1% Triton X-100) with 1% heat-
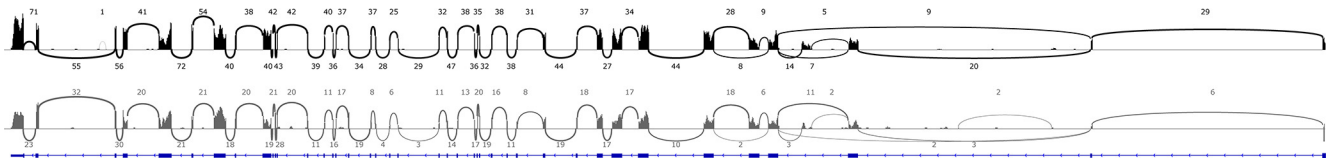
Figure 3. Splicing of *Col6a3* transcripts. Quantification of BPN RNA-seq split reads with two-pass mapping. Numbers indicate number of reads spanning intron indicated by arc. Top, wild-type; bottom, *Col6a3*^CTT/CTT^. Split reads were consistent with expression of a transcript encoding a full-length COL6A3 protein in wild types. In *Col6a3*^CTT/CTT^ mice, exon usage and splicing were indistinguishable from wild type.

inactivated goat serum for 1 h, then incubated with anti-digoxigenin antibody coupled to alkaline phosphatase (Sigma 11093274910, 1:3500) in the same solution overnight. Sections were then washed (10 min/wash) three times in B1 and twice in B2 (100 mM Tris-HCl pH 9, 100 mM NaCl, 50 mM MgCl₂). Sections were then incubated in B2 with 2% nitro blue tetrazolium/5-bromo-4-chloro-3-indolyl-phosphate (NBT/BCIP, Sigma) until adequate color development. The reaction was stopped with B1, and slides were coverslipped with polyvinyl alcohol.

For fluorescent *in situ* hybridization (FISH), sections were fixed in 4% PFA in PBS at 4°C for 1 h, then rinsed twice with PBS. Sections were then dehydrated in ascending concentrations of ethanol (50%, 70%, 100%, 100%; 5 min each). Slides were baked at 37°C for 30 min, then sections were demarcated with a hydrophobic barrier pen. Sections were pretreated with RNAscope Protease IV Reagent (ACD) for 30 min and rinsed twice in PBS. Probes (ACD) were added to sections (C1: *Slc17a7*, C2: *Col6a3*, C3: *Dagla*) and hybridized at 40°C for 2 h. Sections were exposed to amplification reagents (Amp1-FL, 30 min; Amp2-FL, 15 min; Amp3-FL, 30 min; Alt4-FL Alt B, 15 min) at 40°C with two washes of 2 min with RNAscope wash buffer between each step. After 30-s DAPI exposure, sections were coverslipped with Aqua-Poly/Mount (Polysciences, Inc). Images were obtained with an Axio Scan.Z1 digital slide scanner (Zeiss) equipped with a 20× magnification objective. Images were evaluated using the commercially available image analysis software Developer XD 2 (Definiens AG). Thresholds were set empirically for each channel and the same thresholds were applied to all images, allowing nuclei to be classified as positive or negative for each transcript.

For hematoxylin and eosin staining, tibialis anterior muscle was dissected, embedded in OCT (Tissue-Tek), snap frozen in isopentane, and sectioned on a cryostat at 12-μm thickness. Sections were fixed with 4% PFA in PBS for 5 min, then washed in tap water. Next, sections were incubated in Mayer's hematoxylin solution for 5 min, washed with tap water, incubated with 0.5% eosin and 1% acetic acid for 10 min, and washed three times with distilled water. Sections were then dehydrated (70% ethanol for 1 min, 90% ethanol for 30 s, 100% ethanol for 30 s, xylene for 30 s) and coverslipped with Depex. Images of stained muscle sections were captured on a Axio Scan.Z1 digital slide scanner equipped with a 20× magnification objective, and analyzed with FIJI (Schindelin et al., 2012). Transverse fibers were traced using a freehand selection tool by an investigator blinded to the genotype, and measurements of the fiber size (μm²) and circularity (0–1, with 1 = perfect circle and 0.2 = very angular) were recorded.

Genetic engineering
To generate *Col6a3*^CTT^ mice, we linearized the pSpCas9(BB)-2A-Puro (PX459) plasmid (a gift from Feng Zhang; Addgene plasmid #48139) with BbsI and dephosphorylated it with calf intestinal alkaline phosphatase. Guide RNA (gRNA) oligonucleotides (5′-CACCGCACCTCTCG CATCCGGCTGA-3′ and 5′-AAACTCAGCCGGATGCGAGAGGTG C-3′) were simultaneously phosphorylated and annealed as follows:
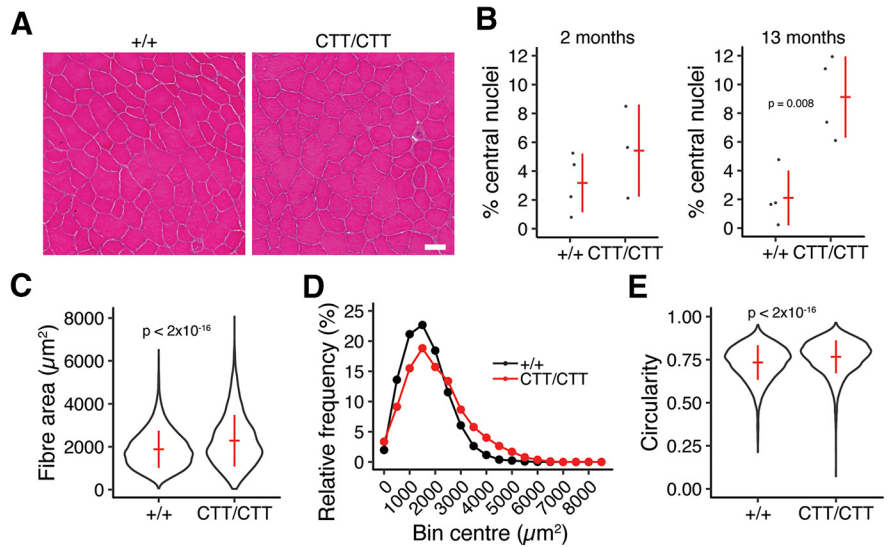

Figure 4. Muscle phenotype of *Col6a3*^CTT/CTT^ mice. *A*, Representative tibialis anterior hematoxylin and eosin staining of tibialis anterior (TA) muscle at 13 months of age. Scale bar: 50 μm. *B*, Proportion of internalized nuclei in TA muscle at age two months (n = 3–4 per genotype) and 13 months (n = 4 per genotype). *C*, *D*, Quantification (*C*) and distribution (*D*) of TA muscle fiber cross-sectional area in 13-month-old mice. *E*, Quantification of circularity of TA muscle fibers in 13-month-old mice. n = 5521–5857 fibers and 4 mice per genotype for *C*–*E*. All error bars are SD and center values are group means. Genotypes were compared by two-sided *t* test.
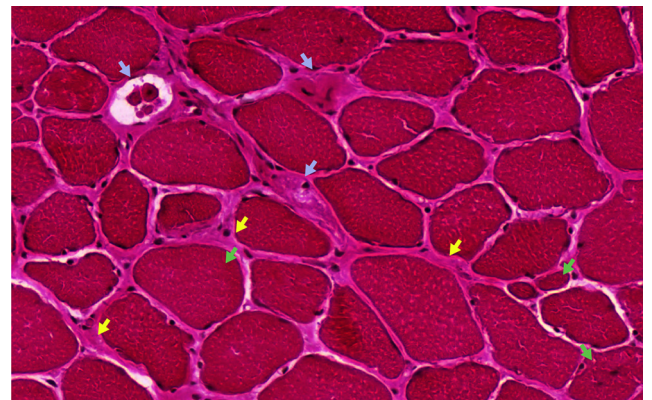
Figure 5. Representative myopathy in aged *Col6a3*^CTT/CTT^ muscle. Hematoxylin and eosin staining of tibialis anterior of 13-month-old *Col6a3*^CTT/CTT^ mouse showing endomysial fibrosis (yellow arrows; increased connective tissue between fibers), fibers at different stages of degeneration/necrosis and regeneration (blue arrows), and rounded fibers with increased size variation and/or internalized nuclei (green arrows).

100 pmol of each oligonucleotide were mixed with T4 ligase buffer and T4 polynucleotide kinase (5 U), and incubated at 37°C for 30 min, 95°C for 5 min, and then cooled to 25°C at a rate of 0.1°C/s. Annealed and phosphorylated oligonucleotides were then ligated into linearized and dephosphorylated PX459 with T4 ligase. Ligation product was transformed into competent bacterial cells, and bacterial clones with successful integration of the gRNA were used for plasmid cloning.
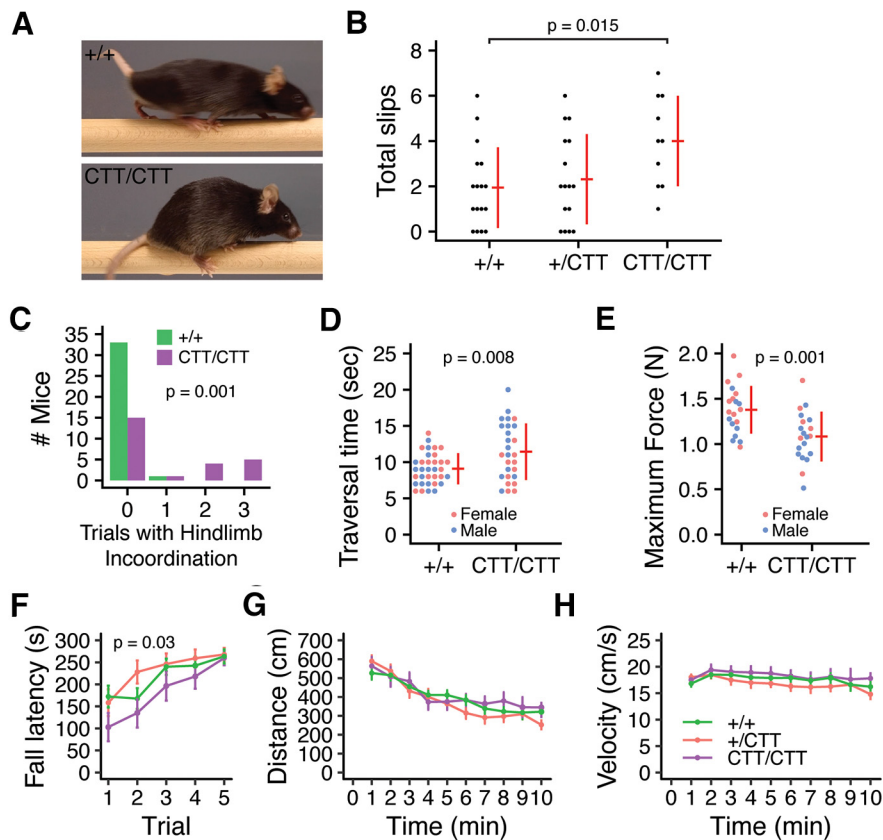
Figure 6. COL6A3 attenuation causes recessive dyskinesia. *A*, Representative images of *Col6a3*$^{+/+}$ and *Col6a3*$^{CTT/CTT}$ mice during beam walk, showing the frame immediately before right forepaw liftoff. *B*, Total hindlimb slips across three beam walk trials (12-mm rectangular beam). Female mice aged seven to eight weeks, $n = 10–17$ per genotype. *C*, Occurrence of hindlimb incoordination across three beam walk trials (12-mm rectangular beam). Male and female mice aged 12–28 weeks, $n = 25–34$ per genotype. *D*, Best traversal time from 3 beam walk trials (12-mm rectangular beam). Male and female mice aged 12–28 weeks, $n = 27–34$ per genotype. *E*, Maximum four limb force in grip strength test. Male and female mice aged 23–29 weeks, $n = 20$ per genotype. *F–H*, Rotarod fall latency on five consecutive trials (*F*); distance traveled (*G*) and velocity (*H*) per minute in activity chamber. Female mice aged seven to eight weeks, $n = 10–17$ per genotype. All error bars are SD and center values are group means. *P* values derived from *t* test, except for *F*, one-way ANOVA between wild types and *Col6a3*$^{CTT/CTT}$. See also Movie 1.
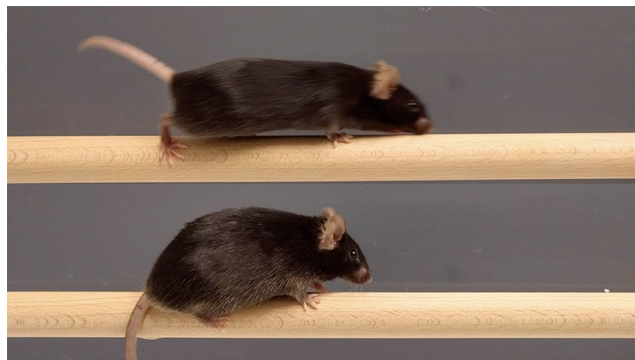

Movie 1. Beam walk performance of *Col6a3*$^{CTT/CTT}$ mice. Representative beam walk performance showing characteristic hindlimb incoordination in *Col6a3*$^{CTT/CTT}$ mice. Top, Wild-type mouse. Bottom, *Col6a3*$^{CTT/CTT}$ mouse with hindlimb incoordination. [View online]

Purified plasmid was transfected into V6.5 mouse embryonic stem (ES) cells with Fugene HD (370-ng plasmid, 100,000 cells). One day after transfection, successfully transfected cells were selected with puromycin (2 µg/ml) for 2 d. Surviving cells were clonally diluted, expanded, and picked for genotyping with the screening primers 5′-AGTGCCCTGTATT CCCAACA-3′ and 5′-AAAGCGTTGATGAGCTGTCG-3′.

In one clone, 5′-CAACTGTCCGCGG-3′ was deleted and replaced by 5′-CCCACAA AGAGAGAGAGTCA-3′, yielding a frame-shift and premature stop codon in exon 36. In the predicted protein product, the 15 amino acid sequence NCPRGARVAVVTYNN is replaced by PQRERVRCPRGCGHL followed by the stop codon, resulting in severe disruption of the C1 domain (out of 180 amino acids, 36 intact, 15 altered, and 129 missing) and complete absence of the C2–C5 domains.

Altered ES cells were injected into blastocysts, which were transferred to the uterus of pseudopregnant female mice. Chimeric offspring were backcrossed to C57/BL6J mice to obtain germline transmission. Mice were genotyped with the primers 5′-AGAGAGCA ACTGTCCGCG-3′ (wild-type-specific sense primer), 5′-AGCCCACAAAGAGAGAGA GT-3′ (CTT-specific sense primer), and 5′-AAAGCGTTGATGAGCTGTC-3′ (common antisense primer) in two separate PCRs (wild-type sense and common antisense primers, yielding a 360-bp product, and CTT-specific sense and common antisense primers, yielding a 367-bp product). The sequence of the CTT allele was verified by RNA-seq (Fig. 3).

We used CRISPOR (Concordet and Haeussler, 2018) to identify potential off-target sites for the guide RNA used. No sites had below four mismatches with the guide sequence. Eleven exonic sites (out of 44 total) had four mismatches. None of the 44 were PAM-adjacent. Of the 11 exonic sites, nine were covered by at least one BPN RNA-seq read extending at least 15 bp in either direction from the PAM. Within these reads, there were no sequence variants.

Quantitative PCR and RNA-seq

Muscle and brain regions were dissected and homogenized (muscle was frozen on dry ice and crushed with a pestle and mortar; brain tissue was homogenized with a syringe and 20-gauge needle in RLT buffer). RNA was extracted with the RNeasy kit (QIAGEN) and reverse transcribed with GoScript Reverse Transcriptase with random primers (Promega). Real-time quantitative PCR was done using FAM-MGB-labeled *Col6a3* (Mm00711678_m1) and *Polr2a* (Mm00839502_m1) TaqMan assays.

For RNA-seq, RNA was prepared as for qPCR. RNA integrity number (RIN) was determined with the Agilent 2100 BioAnalyzer (RNA 6000 Nano kit, Agilent). For library preparation, 1 µg of RNA was poly (A) selected, fragmented and reverse transcribed with the Elute, Prime and Fragment Mix (Illumina). End repair, A-tailing, adaptor ligation and library enrichment were performed as described in the Low Throughput protocol of the TruSeq RNA Sample Prep Guide (Illumina). RNA libraries were assessed for quality and quantity with the Agilent 2100 BioAnalyzer and the Quant-iT PicoGreen dsDNA Assay kit (Life Technologies). RNA libraries were sequenced as 100-bp paired-end runs on an Illumina HiSeq2500 platform. RNA-seq reads were demultiplexed and mapped with STAR (Dobin et al., 2013; version 2.4.2a) to the mm9 genome assembly (UCSC Genome Browser build) using default parameters, except: min length of chimeric segment: 20; quantMode GeneCounts (to quantify reads per gene); 2 pass mapping; unmapped reads kept; all sam attributes output.

Preparation of protein lysates

Tibialis anterior muscles were dissected, frozen on dry ice, and pulverized with a pestle and mortar. Mouse brain lysates were prepared from
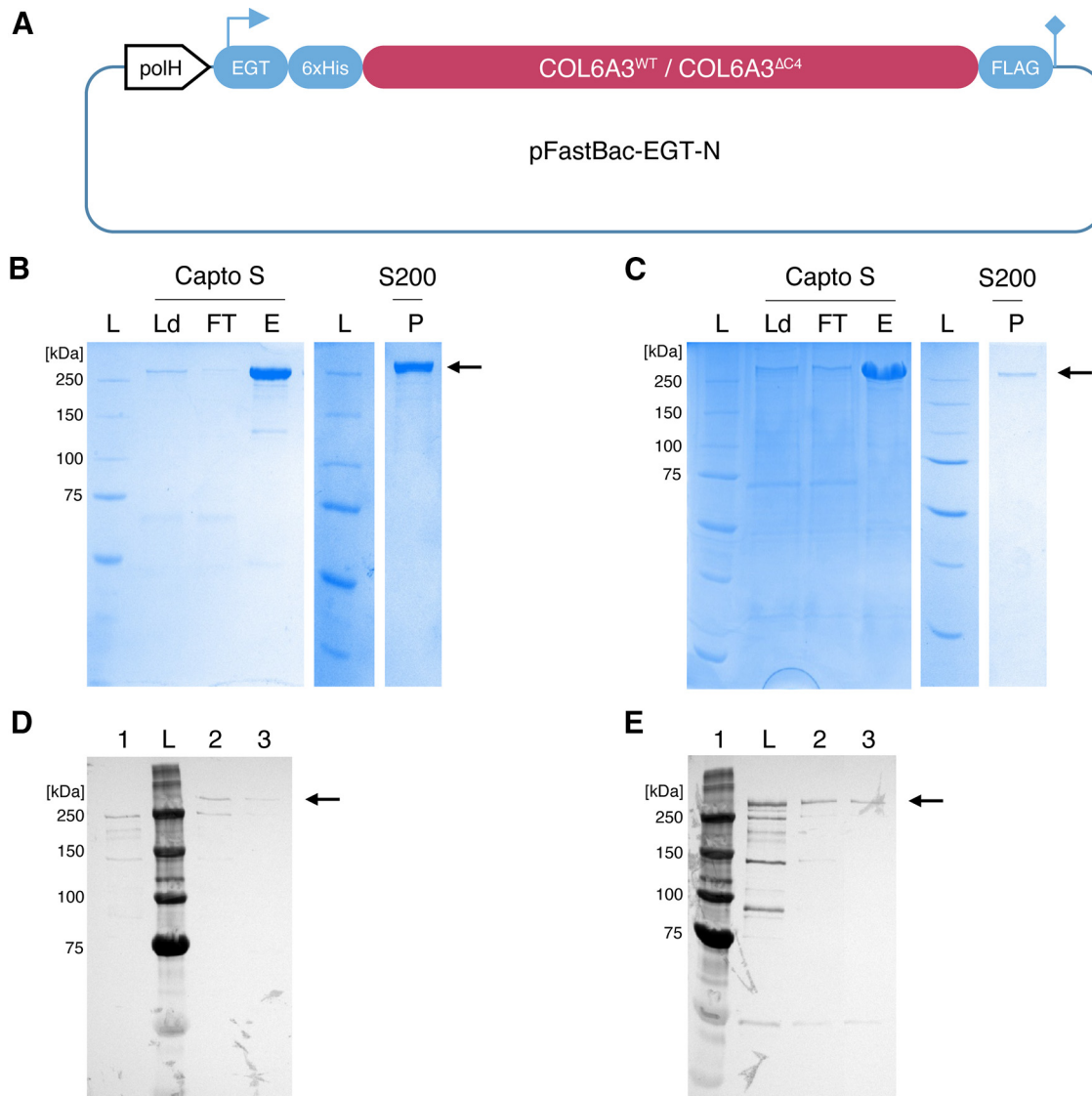
Figure 7. Production of tagged COL6A3 protein. **A**, Schematic overview of the transfer vector pFastBac-EGT-N. COL6A3^{WT} or COL6A3$^{\Delta C4}$ expression is driven by the polyhedrine promoter (polH). The main features include the N-terminal secretion signal ecdysteroid UDP-glucosyltransferase (EGT), N-terminal 6xHis tag, and C-terminal FLAG tag. **B**, **C**, Purification of COL6A3^{WT} (**B**) and COL6A3$^{\Delta C4}$ (**C**) by a two-step strategy. Collagens were captured from culture medium using cation exchange chromatography (CEX) and polished by size-exclusion chromatography (SEC); 15-μl samples of each purification step were subjected to SDS-PAGE and visualized by Coomassie staining. Arrows indicate the presence of COL6A3 with a predicted weight of 290 kDa (COL6A3^{WT}) or 280 kDa (COL6A3$^{\Delta C4}$). Capto S, HiTrap Capto S (CEX); S200, S200pg (SEC); L, protein ladder; Ld, load (growth medium); FT, flow-through; E, elution; P, peak (main protein peak from SEC. **D**, **E**, The success of the two-step purification strategy of COL6A3^{WT} (**D**) and COL6A3$^{\Delta C4}$ (**E**) was further validated by Western blotting using a peroxidase-labeled anti-6xHis antibody; 15-μl samples of each purification step were subjected to SDS-PAGE and Western blotting. Arrows indicate the presence of COL6A3 with a predicted weight of 290 kDa (COL6A3^{WT}) or 280 kDa (COL6A3$^{\Delta C4}$). L, protein ladder; 1, load (growth medium); 2, elution from CEX (HiTrap Capto S); 3, main protein peak from SEC (S200 pg).

fresh microdissected wild-type brain tissue. "LSN+" (Fig. 8B) included also medial septal nucleus and striatum. Dissected tissue was placed in ice cold lysis buffer (150 mM NaCl, 1% NP-40, 50 mM Tris-HCl pH 8, and cOmplete Mini Protease Inhibitor, Merck) and homogenized with a syringe and 20G needle. The sample was agitated at 4°C for 30 min, then centrifuged at 10,000 rpm for 10 min at 4°C. The supernatant (SN) was used for subsequent experiments, with quantification by the DC Protein Assay (Bio-Rad).

Western blottings
We mixed 10 μg of tissue lysate with Laemmli buffer, incubated at 95°C for 5 min, and electrophoresed (SDS-PAGE, 125 V) on 4–20% polyacrylamide gels. Proteins were transferred to nitrocellulose membranes by wet blot, blocked in 5% milk in Tris-buffered saline (TBS) with 1% Tween 20 (TBST) for 1 h, and incubated with primary antibodies [mouse anti-vinculin V9131, Sigma; and from Heumüller et al. (2019) rabbit anti-COL6A3-N 1:500] in TBST with 5% milk at 4°C overnight.

Membranes were washed three times in TBST, then incubated with secondary antibody [horseradish peroxidase (HRP)-conjugated donkey anti-rabbit 406401, BioLegend, 1:1000; HRP-conjugated goat anti-mouse Cay10004302-1, Cayman, 1:1000]. Membranes were again washed three times in TBST, and HRP was chemiluminescently detected with ECL Prime Detection Reagent (GE Healthcare) on a Fusion Pulse imager (Vilber).

Mouse behavioral tests
For the beam walk task, mice were trained to traverse a beam (square profile, 20 mm in diameter, length 90 cm, 15 cm above the surface) with the home cage on one end under normal light. Mice were guided to the home cage if necessary. Mice completed three successive traversals in training. Experiments commenced approximately one week after training. Some mice received injections before testing. The injections were administered in the testing room between 8:30 and 10:30 A.M. Vehicle (0.33% DMSO) or the CB1R agonist WIN 55212-2 (WIN; 1 mg/kg;
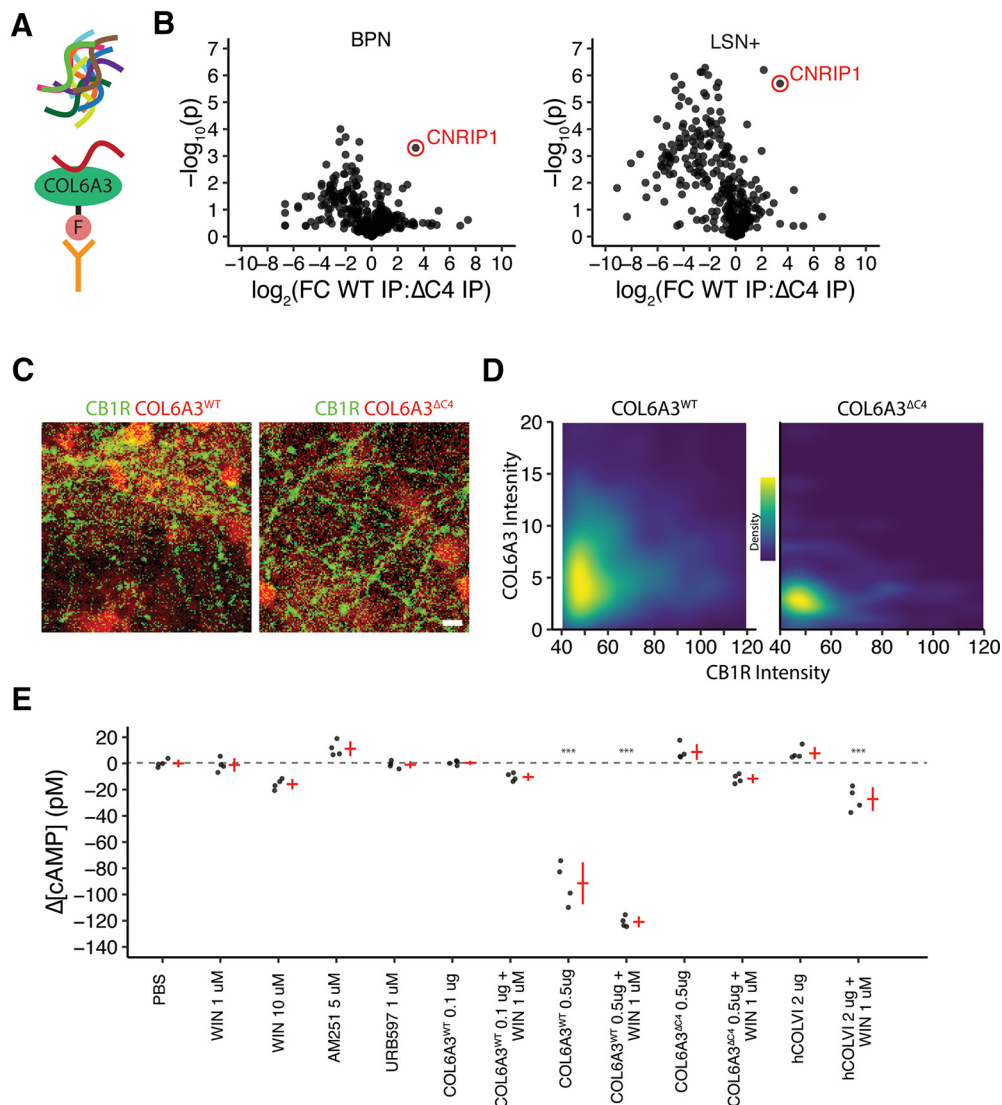
Figure 8. COL6A3 interacts with CB1R. ***A***, Schematic of immunoprecipitation (IP) experiment. FLAG-tagged COL6A3 was conjugated to beads with anti-FLAG antibody, incubated with mouse brain lysates, and eluate was analyzed with mass spectrometry. ***B***, Results of mass spectrometry analysis of IP from BPN and LSN lysates. Each point is a protein. The abscissa is the base 2 logarithm of the ratio of abundance of each protein in the COL6A3^{WT} to COL6A3$^{\Delta C4}$ IP, and the ordinate is the negative base 10 logarithm of the p value comparing the two IPs (two-sided t test, not corrected for multiple comparisons). Proteins toward the top right bind selectively to COL6A3^{WT} compared with COL6A3$^{\Delta C4}$. ***C***, Representative images from wash-and-bind assay on primary mouse cortical neurons showing colocalization (yellow) of COL6A3^{WT} (red) with CB1R (green). Scale bar: 10 μm. ***D***, Pixel-wise density plots of wash-and-bind results, comparing CB1R fluorescence with retention of COL6A3^{WT} or COL6A3$^{\Delta C4}$ (detected by anti-His immunofluorescence). Results are from three technical replicates per condition. ***E***, cAMP assay in mouse primary neurons. COL6A3^{WT}, COL6A3$^{\Delta C4}$, or human collagen VI preparation were added to cells alone or in combination with CB1R agonist WIN. All error bars are SD and center values are group means. P values derived from ANOVA followed by *post hoc* Tukey's HSD test comparing to PBS, ***$p < 0.001$.

Cayman Chemical) were injected intraperitoneally (10 μl/g body weight). Mice in the treatment study received both WIN and vehicle in a randomized crossover design, with the two conditions separated by one to eight weeks; see previous section). Testing commenced 2 h after injection.

In testing, performed under normal light between 10:30 A.M. and 12:30 P.M., mice traversed each of four beams three times each consecutively: 20 mm square profile, 22 mm circular profile, 12 mm square profile, and 15 mm circular profile). The traversal time, number of slips and falls, and the presence of hindlimb incoordination were recorded. Hindlimb coordination was characterized by an apparent inability to coordinate the hindlimbs toward forward locomotion (see Movie 1). The effects of WIN treatment were evaluated separately in mice with baseline values above the overall median for each parameter (impaired mice).

For the grip strength test, maximum grip strength of forelimbs and combined forelimbs and hindlimbs was measured. The mice were allowed to grasp a grid connected to a force sensor (Bioseb) while being

pulled away. Three consecutive trials were conducted for forelimbs and all limbs, and the means of the respective trials were used for analysis.

The rotarod test is designed to evaluate the motor coordination and balance of rodents by forcing the subjects to run. The subjects are placed on a rotating rod (Med Associate Inc, model ENV-575 M) with a steady acceleration and the latency to fall is recorded. The subjects fall safely 16.5 cm below the rotating rod. The experiment consists of 1 d of training and 1 d of testing. On the training day, subjects are placed on the rod accelerating from 2 to 20 rpm for 5 min until they fall or the 5-min trial is complete. This process is repeated for a total of three trials with 15-min intertrial interval (ITI). The subjects receive a resting day after the training day. On the testing day, the mice are tested with constant speed of 16 rpm for a total of 5 trials with 15-min ITI. The rod is cleaned with 1% Virkon between trials.

The Activity Chamber is a simple assessment test used to determine general activity levels, gross locomotor activity, and exploration habits in rodents. Assessment takes place in a square arena, 43.2 × 43.2 cm,
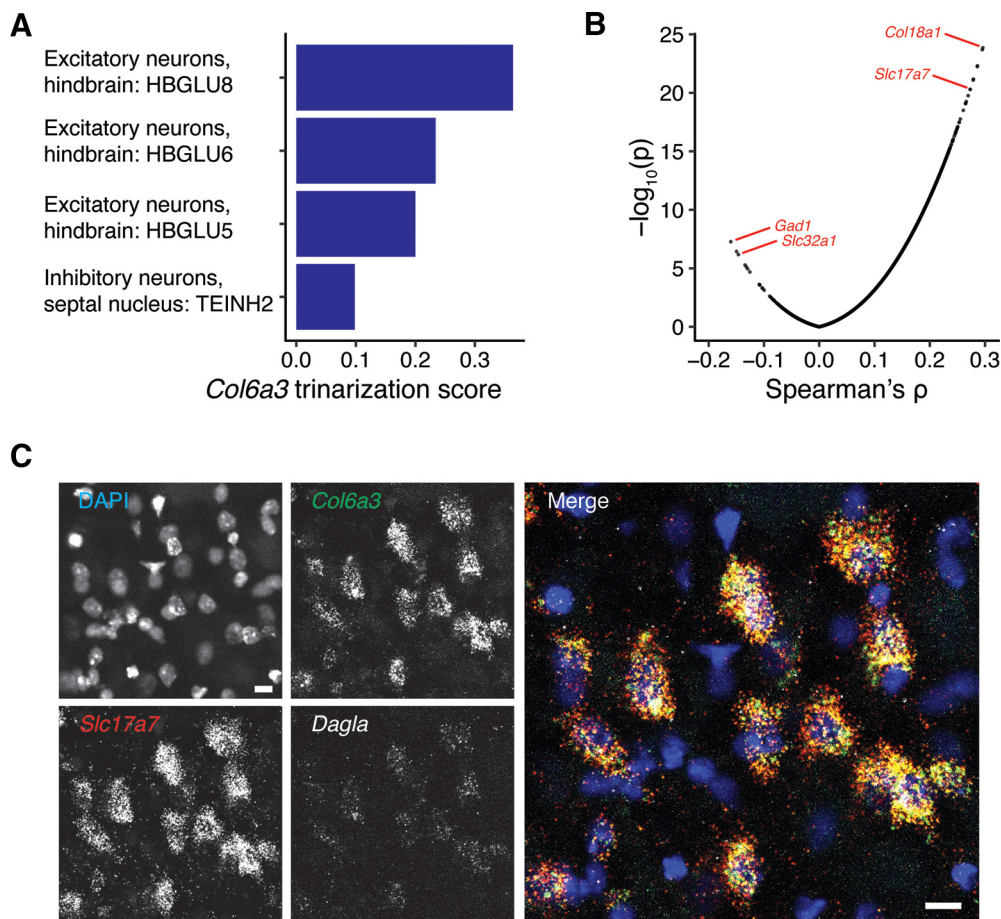
Figure 9. COL6A3 is produced by a distinct pontine cell type. *A*, Ranking of central nervous system cell clusters by *Col6a3* trinarization score (a probabilistic cluster gene expression estimate), using data from Zeisel et al. (2018). *B*, Transcriptome-wide analysis of coexpression with *Col6a3* reveals positive correlation of the glutamatergic neuron marker *Slc17a7* (*Vglut1*) and negative correlation of the inhibitory neuron markers *Gad1* and *Slc32a1* (*Vgat*), indicating that *Col6a3*-expressing cells are glutamatergic neurons. *C*, Triple *in situ* hybridization of adult mouse BPN showing predominant coexpression of *Slc17a7* and the eCB synthesis gene *Dagla* in *Col6a3*-expressing cells. Scale bar: 20 µm.

mounted with three planes of infrared detectors, within a specially designed sound attenuating chamber, 66 × 55.9 × 55.9 cm. The animal is placed in the center of the testing arena and allowed to freely move for 10 min in the dark (with red lighting) while being tracked by an automated tracking system. Distance moved, velocity, jump counts, vertical counts and resting time in the arena are recorded. At the conclusion of each trial the surface of the arena is cleaned with 1% Vikron.

Synthesis of tagged proteins
Mouse COL6A3 sequence without 48 amino acid cleaved leader sequence was amplified by PCR from mouse brain cDNA and cloned into the transfer vector pFastBac-EGT-N (Helmholtz Center Munich) in frame with the N-terminal secretion signal ecdysteroid UDP-glucosyltransferase (EGT), 6xHis tag, and Flag tag. C4 domain sequence was removed with the Q5 site-directed mutagenesis kit (NEB). Mouse prolyl 4-hydroxylase α-chain and β-chain (P4HA1 and P4HB) sequences were amplified by PCR from mouse brain cDNA and cloned into the bicistronic transfer vector pFastBac-Dual (ThermoFisher). Constructs were validated by sequencing before site-specific recombination with the baculovirus genome provided by its host E.coli strain DH10Bac (Bac-to-Bac-System, Invitrogen). Positive recombinant clones were identified by blue-white screening and further confirmed by PCR. Recombinant viral DNA was extracted under alkaline conditions, followed by ethanol precipitation (Birnboim and Doly, 1979) and used for transfection into insect cells (FuGENE HD, Promega). Baculovirus recombinant for COL6A3^{WT} or COL6A3$^{\Delta C4}$ was propagated in Sf21 cells, and SN was kept at 4°C for further analysis and protein production. Low passage viral titer was determined by quantitative PCR (Lo and Chao, 2004). Briefly, viral DNA was purified from SN (High Pure Viral Nucleic Acid

kit, Roche) and PCR was set up with Brilliant II qPCR Low ROX Master Mix (Agilent Technologies). qPCR reaction and data were acquired on an Agilent Mx3005P qPCR System.

COL6A3^{WT} and COL6A3$^{\Delta C4}$ were produced in High Five insect cells. For protein production, High Five cells were seeded 1 d before infection at 1×10^{6} cells/ml in InsectXpress medium (Lonza). Cells were co-infected with low-passage recombinant baculovirus for COL6A3^{WT} or COL6A3$^{\Delta C4}$ along with P4HA1/P4HB at a MOI of 2 and 0.2, respectively, in the presence of 80 µg/ml ascorbic acid (AppliChem). Cells were incubated at 21°C on an orbital shaker. SN was harvested 3 d postinfection by centrifugation, adjusted to final concentrations of 20 mM Tris pH 7.1 and 0.02% thioglycerol (TG), and filtered (0.45 µm Stericup, Merck Millipore). Collagens were captured by ion exchange chromatography using a CaptoS-5 ml prepackaged column (GE Healthcare) and eluted with 20 mM Tris pH 7.1, 0.02% TG, and 250 mM NaCl. Positive fractions were pooled, concentrated (Amicon, 30-kDa MWCO, Merck Millipore) and polished by gel filtration using an S200pg (GE Healthcare) buffered in 20 mM Tris pH 7.1, 0.02% TG, and 300 mM NaCl. Positive fraction were pooled, concentrated and lyophilized in aliquots. Purity was determined by SDS-PAGE and Coomassie staining (Page Blue, Fermentas), and protein concentration was determined photometrically. Purified tagged COL6A3 proteins are depleted, but plasmids to produce them are freely available from the authors.

Immunoprecipitation
For identification of COL6A3 binding partners, anti-FLAG M2 magnetic beads (Merck) were used; 20-µl beads were diluted in 100 µl TBS for each immunoprecipitation reaction. The beads were washed three times with TBS, then incubated with an empirically optimized 4 µg of FLAG-tagged COL6A3 protein in TBS with agitation for 1 h at room
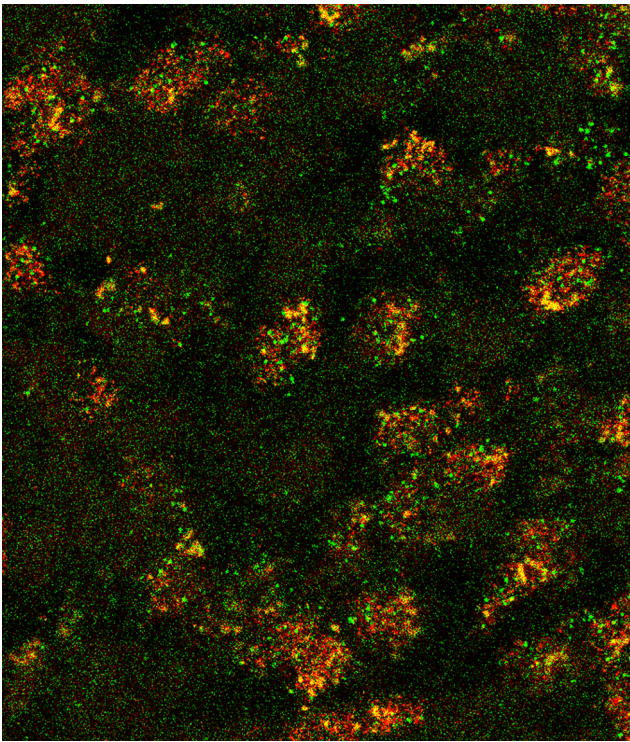
Figure 10. RNAscope specificity. Representative BPN RNAscope image showing *Dagla* in green and *Col6a3* in red.

temperature. The beads were again washed three times with TBS. Bait-bound beads were then incubated with an empirically optimized 250 µg of brain lysate in a volume of 1 ml with agitation at room temperature for 2 h. The beads were again washed three times with TBS. Bait-bound proteins were eluted from the beads with Laemmli buffer (80 mM Tris-HCl pH 6.8, 2% SDS, 10% glycerol, 5% ß-mercaptoethanol, and 0.02% bromophenol blue) at 95°C for 5 min.

Sample preparation for liquid chromatography-mass spectrometry (LC-MSMS) analysis

For identification of COL6A3 binding partners, Laemmli eluates were subjected to a modified filter-aided sample preparation (FASP) procedure as described (Wiśniewski et al., 2009; Grosche et al., 2016). Briefly, proteins were diluted in ammonium bicarbonate before reduction and alkylation using dithiothreitol and iodoacetamide. Urea was added to a final concentration of 4 M, followed by centrifugation of denatured proteins on a filter device (Sartorius, Vivacon 500). After several washing steps with 8 M urea and ammonium bicarbonate, proteins were subjected to on-filter proteolysis with Lys-C (Wako Chemicals) and trypsin (Promega). Tryptic peptides were eluted by centrifugation and acidified with trifluoroacetic acid before LC-MSMS analysis.

For whole proteome analysis of wild-type versus *Col6a3*[CTT/CTT] brain tissue, equal amounts of ground brain tissue were lysed in 8 M urea in 0.1 M Tris-HCl pH 8.5 using the Precellys 24 tissue homogenizer (Bertin Instruments). Crude lysates were subjected to FASP digest as described above.

Quantitative LC-MSMS analysis

Digested IP samples were measured in data-dependent acquisition mode on a Q-Exactive HF mass spectrometer (Thermo Fisher Scientific) online coupled to an Ultimate 3000 RSLC (Dionex, part of Thermo Fisher Scientific). Peptides were trapped on a C18 precolumn cartridge before separation on a nanoEase MZ HSS T3 Column (100 Å, 1.8 µm, 75 µm × 250 mm, Waters) in a nonlinear acetonitrile gradient over 95 min. Both the precursor (scan range 300–1500 m/z) and TOP10 MS2 spectra of charges 2–7 were acquired in the orbitrap mass detector of the mass spectrometer, at resolutions of 60,000 and 15,000, respectively.

Maximum injection times were set to 50 ms for MS and MS2 scans and dynamic exclusion to 30 s. Acquired raw files were analyzed in the Progenesis QI software for MS1 intensity based label-free quantification (version 3.0, Nonlinear Dynamics, Waters) as described previously (Hauck et al., 2010; Frik et al., 2018). MSMS spectra were searched against the Swissprot mouse database (16,868 sequences, release 2017_02) using the Mascot search engine (Matrix Science). Search settings were: enzyme trypsin, 10 ppm peptide mass tolerance and 0.02-Da fragment mass tolerance, one missed cleavage allowed, carbamidomethylation was set as fixed modification; methionine oxidation and asparagine or glutamine deamidation were set as variable modifications. Applying the mascot percolator algorithm (Brosch et al., 2009) resulted in a peptide false discovery rate of 0.49%. The abundances of all unique peptides per protein were summed. Resulting normalized abundances of the individual proteins were used for calculation of fold changes and significance values by Student's *t* test.

Whole proteome analysis of wild-type versus *Col6a3*[CTT/CTT] brain tissue was performed in data-independent acquisition mode on the LC-MSMS setup described above, as described previously (Lepper et al., 2018; Mattugini et al., 2018). MS spectra from 300–1650 m/z were recorded at 120,000 resolution with an AGC (automatic gain control) target of 3×10^6 and a maximum injection time of 120 ms. The mass range was divided into 37 data-independent acquisition windows of unequal size based on previous data-dependent acquisition runs, with each a scan resolution of 30,000 and an AGC target of 3×10^6. Generated raw files were analyzed using the Spectronaut X software (Biognosys; Bruderer et al., 2015) employing an in-house mouse spectral meta-library which was generated using Proteome Discoverer 2.1 (Thermo Fisher Scientific), Byonic search engine (Protein Metrics) and the Swissprot mouse database (release 2017_02). Quantification was based on the sum of MS2 area levels of all unique peptides per protein fulfilling the *q* value percentile 0.25 setting with a maximum peptide false discovery rate of 1%. Resulting protein abundances were again used for calculation of fold changes and significance values by Student's *t* test.

Primary mouse cortical neurons

Cortices of newborn mice were dissected and placed in ice cold HBSS supplemented with 20% fetal bovine serum, 4.2 mM NaHCO$_3$, and 1 mM HEPES. Tissue was washed three times in HBSS, then incubated with papain (Neuron Isolation Enzyme, Thermo Fisher Scientific) at 37°C for 15 min. Digested tissue was then washed three times in HBSS and three times in plating medium (Neurobasal-A with GlutaMax, B27, and penicillin-streptomycin). DNase I (0.05 U/µl) was added to the final wash. Tissue was then triturated, filtered through a 40 µm strainer, and plated on poly-D-lysine-coated coverslips at 250,000 cells per cm^2.

Wash and bind assay

Mouse primary neurons at 2 days in vitro (DIV) were used. COL6A3[WT] or COL6A3[ΔC4] were added (1 µg per well of 24-well plate, *n* = 3 replicates per condition) and incubated for 2 h at 37°C. Cells were then washed five times with PBS, fixed with 4% PFA for 15 min, and labeled with 6×-His Tag Antibody coupled to Alexa 555 (Thermo Fisher Scientific, MA1-21315-A555). Coverslips were mounted on slides (Aqua-Poly/Mount) and images obtained while blinded to condition with a LSM880 confocal microscope (Zeiss) equipped with a 20× magnification objective.

cAMP assay

Mouse primary neurons at 2 DIV were used, and the cAMP-Glo Max Assay (Promega) was used for cAMP detection and quantification. The induction medium consisted of PBS with 500 *µ*M 3-isobutyl-1-methylxanthine (IBMX), 100 *µ*M Ro-20-1724, 10 *µ*M forskolin, and 40 mM MgCl$_2$. Cells were incubated with induction medium and test compounds for at 37°C for 15 min. Samples were then analyzed using the manufacturer's luminescence protocol.

Single-cell RNA-seq analysis

Cluster trinarization scores are as provided by the authors (Zeisel et al., 2018). We used the full set of hindbrain neurons from Zeisel et al. (2018;
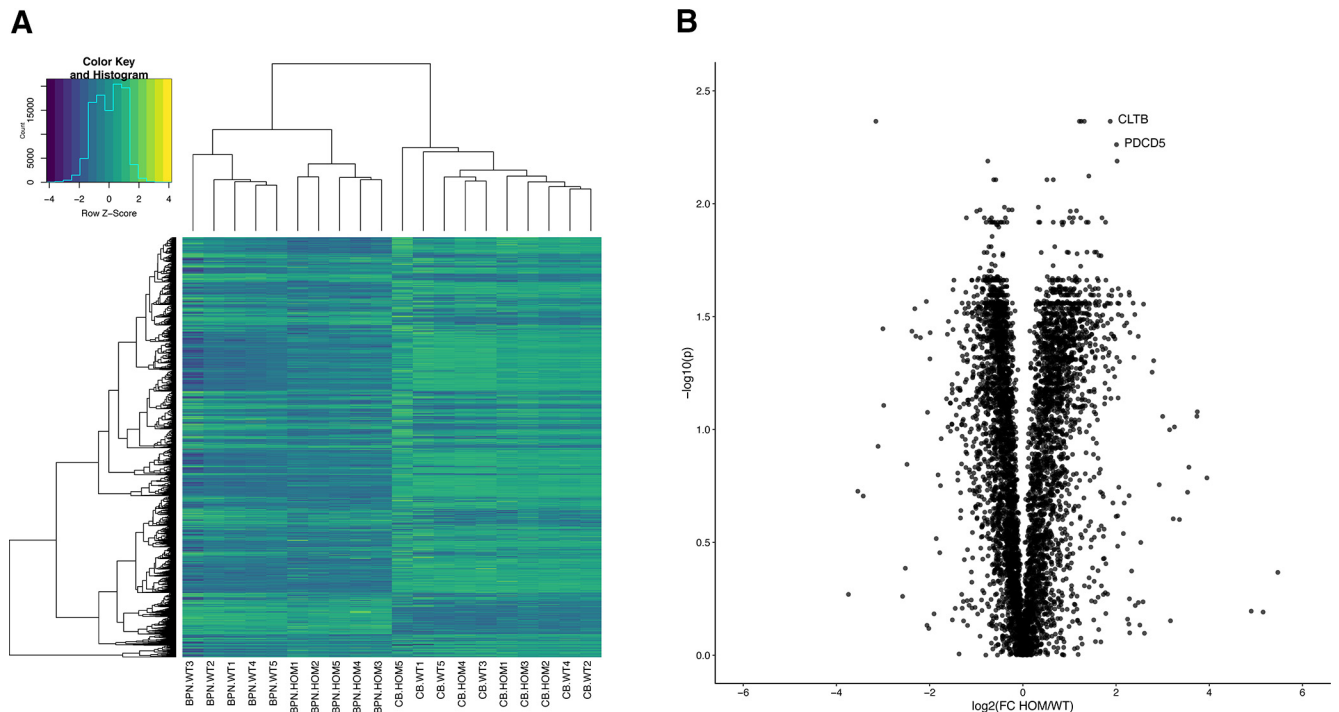
A

B

Figure 11. Proteomic analysis of *Col6a3*^CTT/CTT brain tissue. *A*, Hierarchical clustering of 5609 proteins detected my LC-MSMS in BPN and cerebellar (CB) tissue of wild-type (WT) and *Col6a3*^CTT/CTT mice (HOM). Genotype clearly separated the samples in the BPN but not CB. *B*, Volcano plot of the BPN proteins, showing genotype differences. CLTB (clathrin B) and PDCD5 (programmed cell death 5) are highlighted. *P* values were adjusted by the false discovery rate method.

"L6_Hindbrain_neurons.loom"). This dataset contained 1144 cells, of which 97 expressed Col6a3. We performed gene-wise Spearman correlation in R (cor.test) using all 1144 hindbrain neurons and all 27,998 genes.

Electrophysiology

We prepared coronal brain slices (200 μm) in ice-cold, oxygenated (95% O_2, 5% CO_2) sucrose-based artificial CSF (aCSF) containing the following: 250 mM sucrose, 2.5 mM KCl, 1.24 mM NaH_2PO_4, 10 mM $MgCl_2$, 10 mM glucose, 26 mM $NaHCO_3$, and 0.5 mM $CaCl_2$ (305 mOsm/l). We then incubated slices in ACSF containing the following: 124 mM NaCl, 2.5 mM KCl, 1.24 mM NaH_2PO_4, 1.3 mM $MgCl_2$, 10 mM glucose, 26 mM $NaHCO_3$, and 2.5 mM $CaCl_2$ (300 mOsm/l) at 37°C for 15 min. Thereafter, slices were bisected and maintained and recorded at 22°C, with an aCSF flow rate of ~1.5 ml/min.

For current-clamp recordings and voltage-clamp recordings, the internal pipette solution contained the following: 130 mM K-gluconate, 2 mM KCl, 3 mM $MgCl_2$, 2 mM MgATP, 0.2 mM Na_2GTP, 10 mM HEPES, and 1 mM EGTA (290 mOsm/l, pH 7.25). To measure spontaneous IPSCs (sIPSCs) activity, the internal pipette solution contained the following: 140 mM KCl, 10 mM HEPES, 1 mM EGTA, 5 mM MgATP, 3.3 mM $MgCl_2$, and 0.3 mM NaGTP (290 mOsm/l, pH 7.25), with 1 mM kynurenic acid added to the aCSF. 0.01% Neurobiotin was included within the pipette solutions for postprocessing.

All recordings were acquired with a HEKA EPC10 USB and PATCHMASTER software (HEKA). Voltage-clamp recordings were low pass filtered at 3 kHz and sampled at 7 kHz, while current-clamp recordings were filtered at 10 kHz and sampled at 20–25 kHz. We monitored changes in input resistance (R_{in}) during the course of the experiments by periodically injecting hyperpolarizing steps (-20 pA or -40 pA) in current-clamp mode. Cells were excluded from analysis if R_{in} deviated by >20% over time. For current-clamp recordings, BPN neurons were recorded at their resting membrane potential (RMP). For voltage-clamp recordings, V_h was -60 mV. Membrane potential measurements were not corrected for the liquid junction potential between pipette solution and the recording chamber. The reference electrode was a Ag/AgCl⁻ pellet. Only one BPN neuron per slice was recorded during pharmacology

experiments. For postpatch processing, slices were fixed overnight in 4% PFA, washed three times in PBS, mounted on SuperFrost slides, and coverslipped with VECTASHIELD mounting medium with DAPI (Vector Laboratories).

Quantification and statistical analysis

In the beam walk task, hindlimb slips were counted manually and traversal time measured by a stopwatch by observers blinded to genotype and treatment. Hindlimb incoordination was likewise evaluated by blinded observers, rated as either present or absent (not graded). For behavioral data and muscle histology, two-way group comparisons were evaluated by two-sided *t* test; within-subjects comparisons were evaluated by paired *t* test. Results of the wash-and-bind assay were analyzed by extracting pixel intensity values in each channel for each image (ImageJ). Pixels were thresholded (CB1R intensity >40) and pixel-wise CB1R-COL6A3 intensity correlations were compared between COL6A3^WT and COL6A3^ΔC4 groups by Fisher's z transformation. For the cAMP assay, the effect of treatment was assessed with ANOVA followed by *post hoc* Tukey's HSD test for intergroup comparisons.

Patch-clamp recording data were analyzed using Clampfit 10 (Molecular Devices) and MiniAnalysis (Synaptosoft). Sample traces were generated with Igor Pro v6 (WaveMetrics) and graphs produced with Prism 7 (GraphPad) or the ggplot2 R package. The nonparametric Kolmogorov–Smirnov test (K–S test; MiniAnalysis) was used to quantify the effects of bath applied pharmacological treatments on each neuron before grouping the data. To compare basal EPSC and IPSC events between genotypes, and the effects of pharmacological interventions, 200 events per neuron per time period in question were used for analysis. To assess effects of pharmacological interventions on voltage-clamp recordings, cells were included for statistical analysis if the peak current was greater than the mean ± 2*SD of the preceding baseline value. Baseline values were taken from a minimum period of 4 min before intervention, in 30-s bins. These data were then used to calculate the average frequency, amplitude, and the response compared with baseline (Δ) over time. Unless otherwise stated, data are presented as mean ± SEM with the number of cells per group represented in parentheses for figures comparison of pharmacological interventions on the same
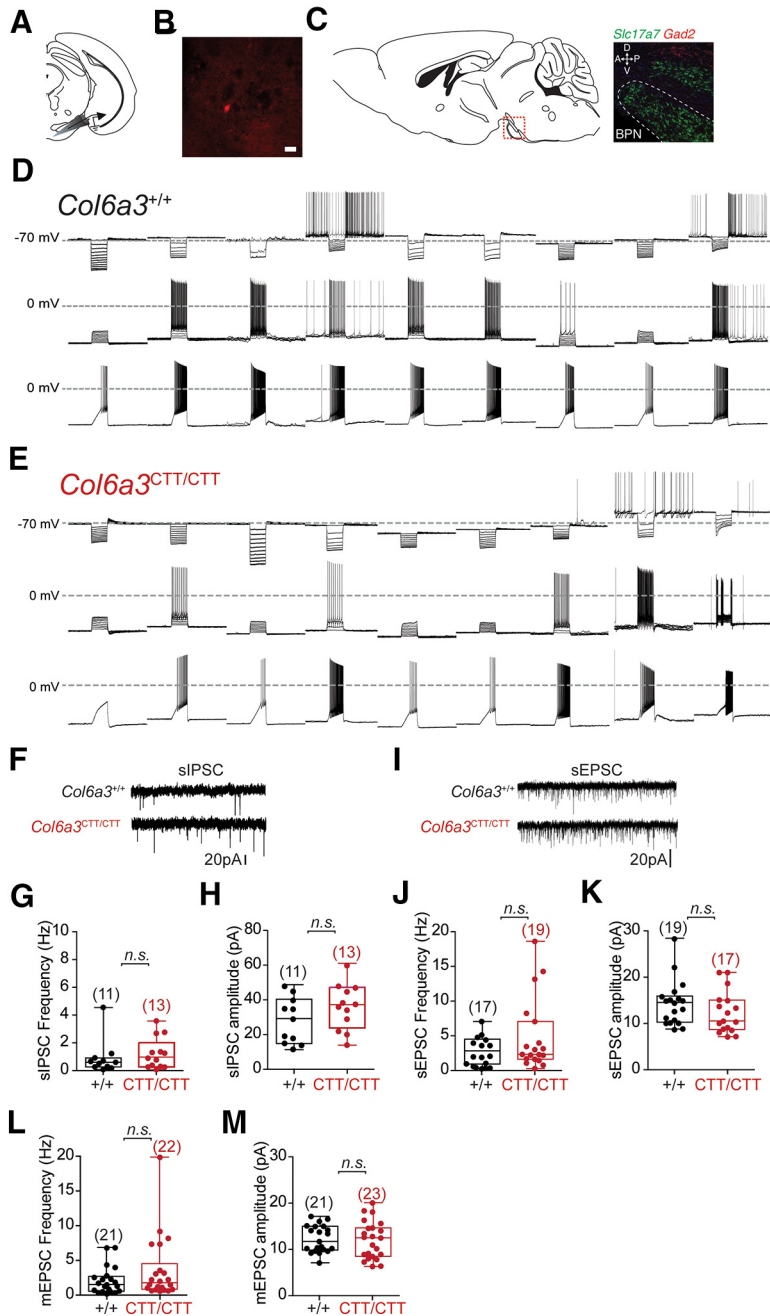
Figure 12. Intrinsic properties of BPN neurons. **A**, Location of patch clamp recordings. Schematic of coronal brain section with targeted region indicated with electrode. **B**, Example of patched BPN neuron. The recorded cell was filled with neurobiotin and immunolabeled with streptavidin-Alexa Fluor 594. Filled cell visible in red. Scale bar: 20 μm. **C**, BPN cell type. Left, Schematic sagittal section with red box indicating position of detail. Right, In situ hybridization showing *Slc17a7* (glutamatergic neuron marker) in green, *Gad2* (GABAergic neuron maker) in red, and DAPI (nuclei) in blue. All BPN neurons are glutamatergic. **D**, **E**, Representative current-clamp recordings of different wild-type (**D**) and *Col6a3*^CTT/CTT (**E**) BPN neurons showing mixture of spontaneously firing and silent cells and their responses to current injection (top rows: −20-pA steps; second rows: +10-pA steps; bottom rows: +200-pA ramp). Each column is from the same cell. **F**, Representative voltage-clamp recordings of wild-type and *Col6a3*^CTT/CTT BPN neurons showing sIPSCs. **G**, **H**, sIPSC frequency (**G**) and amplitude (**H**). **I**, Representative voltage-clamp recordings of wild-type and *Col6a3*^CTT/CTT BPN neurons showing sEPSCs. **J**, **K**, sEPSC frequency (**J**) and amplitude (**K**). **L**, **M**, mEPSC frequency (**L**) and amplitude (**M**). See also Extended Data Figure 12-1.

neuron were analyzed using paired *t* tests; different groups of cells were compared using unpaired two-sided *t* tests. For experiments where data were collected repeatedly for each cell, repeated measures (RM)-ANOVA was used. A statistical significance threshold of $p < 0.05$ was used.

Results

Domains and expression of COL6A3

Collagen $\alpha3$ (VI), or COL6A3, consists of globular N-terminal domain and CTD, which are divided into subdomains (N1–10 and C1–5) on the basis of structural motifs, and a collagenous, or triple helical, domain (Fig. 1A). Uniquely among collagen VI subunits, COL6A3 contains a fibronectin Type III C4 domain (Bonaldo and Colombatti, 1989), which is affected by the majority of dystonia-related variants (Zech et al., 2015; Fig. 1B). Indeed, each of the *COL6A3*-related dystonia families harboured at least one deleterious variant in the portion of this domain encoded by exon 41 (Zech et al., 2015; Fig. 1B). In contrast, Bethlem and Ullrich myopathy-related variants almost exclusively affect the N-terminal and collagenous domains (Fig. 1B).

Given the paucity of information, we asked whether *Col6a3* is expressed in the brain. In situ hybridization experiments in mouse brain revealed that *Col6a3* expression is highly restricted and is only found in two notable clusters, in the lateral septal nucleus (LSN) and the BPN (Figs. 1C,D).

COL6A3 attenuation causes recessive dyskinesia

To delineate the function of the COL6A3 CTD, which is selectively affected in dystonia patients, we generated COL6A3 C-terminal truncation (*Col6a3*^CTT) mice. To that end, we inserted a premature stop codon into exon 36, encoding the C1 domain (Fig. 2A). This mutation, verified at the RNA level (Fig. 2B), is expected to result in a truncated COL6A3 protein lacking the majority of the CTD. Both heterozygous and homozygous *Col6a3*^CTT mice were born in Mendelian ratios, were viable and fertile, and did not show any gross morphologic abnormalities.

COL6A3 expression was reduced in *Col6a3*^CTT/CTT mice, presumably because of nonsense-mediated decay (Fig. 2C–H). Based on RNA-seq analysis, wild-type mice express an mRNA encoding full-length COL6A3 in the BPN, where expression is ~25% of the level of tibialis anterior muscle (Figs. 2D, 3). COL6A3 protein levels generally reflected mRNA levels (Fig. 2H). In *Col6a3*^CTT/CTT mice, exon usage and splicing were indistinguishable from wild-type (Fig. 3). At age two months, *Col6a3*^CTT/CTT mice show no overt (but possibly incipient) muscle pathology, while older mice develop a degenerative myopathy of modest severity (Figs. 4, 5). Specifically, two-month-old mice show no significant change in the proportion of internalized nuclei, a sign of damaged myofibers (Folker and Baylies, 2013). In contrast, 13-month-old mice had more internalized nuclei (Welch's *t* test: $p = 0.008$, $t = -4.1$, df = 5.3) and greater variability in myofiber size and shape, indicative of ongoing degeneration (Fig. 5).

Upon behavioral characterization, *Col6a3*[CTT] mice showed a marked recessive dyskinetic phenotype, characterized in the beam walk test by increased slips (wild-type 1.9 ± 0.4 slips; *Col6a3*[CTT/CTT] 4.0 ± 0.6 slips; Welch's *t* test: $p = 0.015$, $t = -2.7$, df = 17.3; Figs. 6A,B), profound hindlimb incoordination (wild-type 0.03 ± 0.03 trials; *Col6a3*[CTT/CTT] 0.96 ± 0.25 trials; Welch's *t* test: $p = 0.001$, $t = -3.6$, df = 24.6; Fig. 6C; Movie 1), and slower traversal speed (wild-type 9.0 ± 0.4 s; *Col6a3*[CTT/CTT] 11.4 ± 0.8 s; Welch's *t* test: $p = 0.008$, $t = -2.8$, df = 38.3; Fig. 6D). The recessive nature of the phenotype accords with the recessive inheritance pattern of dystonia caused by COL6A3 CTD variants in humans (Zech et al., 2015). *Col6a3*[CTT/CTT] (homozygous) mice produced less grip strength than wild types (wild-type 1.4 ± 0.1 N; *Col6a3*[CTT/CTT] 1.1 ± 0.1 N; Welch's *t* test: $p = 0.001$, $t = 3.5$, df = 37.9; Fig. 6E). *Col6a3*[CTT] mice also showed a significant recessive impairment on the rotarod (Fig. 6F), while locomotor performance (distance and speed) were not impaired (Figs. 6G, H). The behavioral phenotype was consistent across different ages, laboratories, and assessors. One cohort of females aged seven to eight weeks was characterized at the Stanford Behavioral and Functional Neuroscience Laboratory, where total slips on the 12-mm beam were 1.9 ± 0.4 slips for wild types and 4.0 ± 0.6 for *Col6a3*[CTT/CTT]; $p = 0.0015$). Another cohort of males and females aged 12–28 weeks was characterized at the Helmholtz Center Munich, where the corresponding values were 1.0 ± 0.2 slips for wild types and 2.2 ± 0.5 for *Col6a3*[CTT/CTT]; Welch's *t* test: $p = 0.03$, $t = -2.2$, df = 40.1).

COL6A3 interacts with CB1R
To identify binding partners of the COL6A3 C4 domain, the domain most impacted by dystonia variants, we performed an unbiased protein interaction screen. We first synthesized full-length wild-type murine COL6A3 (COL6A3[WT]) and COL6A3 with the C4 domain deleted (COL6A3[ΔC4]). The proteins were synthesized using baculovirus in insect cells (Fig. 7). As proline hydroxylation is critical for posttranslational folding and normal conformation of collagen molecules (Chopra and Ananthanarayanan, 1982; Vitagliano et al., 2001), we concomitantly expressed proline hydroxylase. The proteins were then coupled to beads and incubated with mouse brain lysates followed by mass spectrometry of the bead eluate (Fig. 8A).

Using both BPN and LSN lysates from microdissected mouse brains, this approach identified the cannabinoid receptor interacting protein CNRIP1 as preferentially binding to the C4 domain of COL6A3 (Fig. 8B). As membrane proteins are difficult to access with detergent solubilization, we surmised that this association occurs between the extracellular COL6A3, the membrane-integral CB1R, and the intracellular CNRIP1.

To independently confirm the COL6A3-CB1R interaction, we performed wash-and-bind assays in primary cortical neurons, showing that COL6A3 binding was positively correlated with extent of CB1R expression (Fig. 8C,D). We computed Pearson's correlations between COL6A3 (WT or ΔC4) and CB1R fluorescence for each pixel and obtained r^2 values of 0.05 for COL6A3[WT] and -0.006 for COL6A3[ΔC4]. Comparison of these correlations by Fisher's z transformation revealed a significant effect of C4 domain deletion on the correlation of CB1R fluorescence with COL6A3 retention, indicating that the retention of COL6A3[ΔC4] by CB1R was significantly reduced compared with COL6A3[WT] ($p = 0.02$).

Finally, we showed that COL6A3[WT], but not COL6A3[ΔC4], synergized with CB1R agonist WIN to reduce cAMP levels (Fig. 8E). Specifically, the effect of $0.5 \mu g$ COL6A3[WT] + WIN was
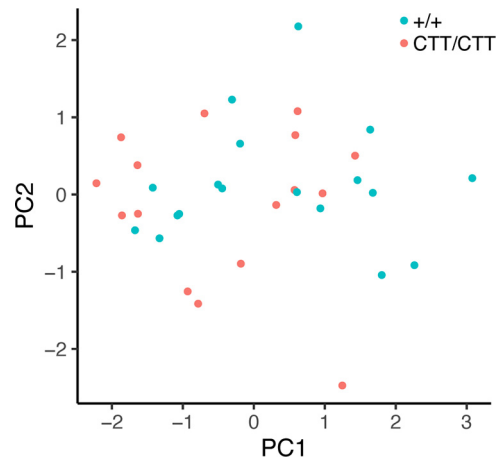

Figure 13. Principal component analysis of current clamp data. Principal component analysis was performed using action potential threshold, action potential adaptation (difference between first and last interspike interval), and input resistance as parameters.

greater than for COL6A3[WT] alone (ANOVA with *post hoc* Tukey's HSD test, $p = 0.0001$). The effect of a human collagen VI preparation was also greater with WIN than without (ANOVA with *post hoc* Tukey's HSD test, $p = 3 \times 10^{-6}$).

COL6A3 is produced by a distinct pontine cell type
To determine COL6A3-expressing cell types, we harnessed a recently published single cell RNA sequencing catalog of mouse nervous system cells (Zeisel et al., 2018). The central nervous system cell clusters with the highest *Col6a3* trinarization score, a probabilistic estimate of gene expression in cell types, were excitatory brainstem neurons mapping to the BPN and inhibitory neurons of the septal nucleus (Fig. 9A). These results independently confirm our *in situ* hybridization findings (Fig. 1C,D). Within the 97 hindbrain neurons expressing *Col6a3*, expression of *Col6a3* was positively correlated with the excitatory neuron marker *Slc17a7* (Vglut1) and negatively correlated with the inhibitory neuron markers *Gad1* and *Slc32a1* (Vgat; Fig. 9B), indicating that *Col6a3* expression is specific to excitatory neurons over inhibitory neurons. *In situ* hybridization confirmed that BPN *Col6a3*-expressing cells predominantly co-express the glutamatergic neuron marker *Slc17a7* ($89 \pm 3\%$, $n = 3$; Fig. 9C). BPN *Col6a3*-expressing cells also predominantly co-express *Dagla* ($84 \pm 4\%$, $n = 3$; Figs. 9C, 10), which encodes diacylglycerol lipase α, the catalytic enzyme for biosynthesis of the eCB 2-arachidonoylglycerol (2-AG). With the caveat that RNA expression does not confirm protein expression, we conclude that BPN glutamatergic neurons can synthesize both collagen VI and 2-AG.

COL6A3 truncation impairs plasticity of pontine afferents
Since COL6A3 interacts with CB1R, which mediates synaptic downscaling *via* retrograde inhibition (Wilson and Nicoll, 2001), we hypothesized that COL6A3 truncation may affect synaptic plasticity. Specifically, we hypothesized that COL6A3 truncation would perturb long-term synaptic depression mediated by CB1R (Robbe et al., 2002; Chevaleyre and Castillo, 2003; Kreitzer and Malenka, 2007). We reasoned that collagen VI would, analogous to collagen IV, affect afferent axons at the site of collagen secretion (Xiao and Baier, 2007; Xiao et al., 2011). Further justifying the assumption that collagen VI is secreted locally, the *Col6a3*[CTT/]
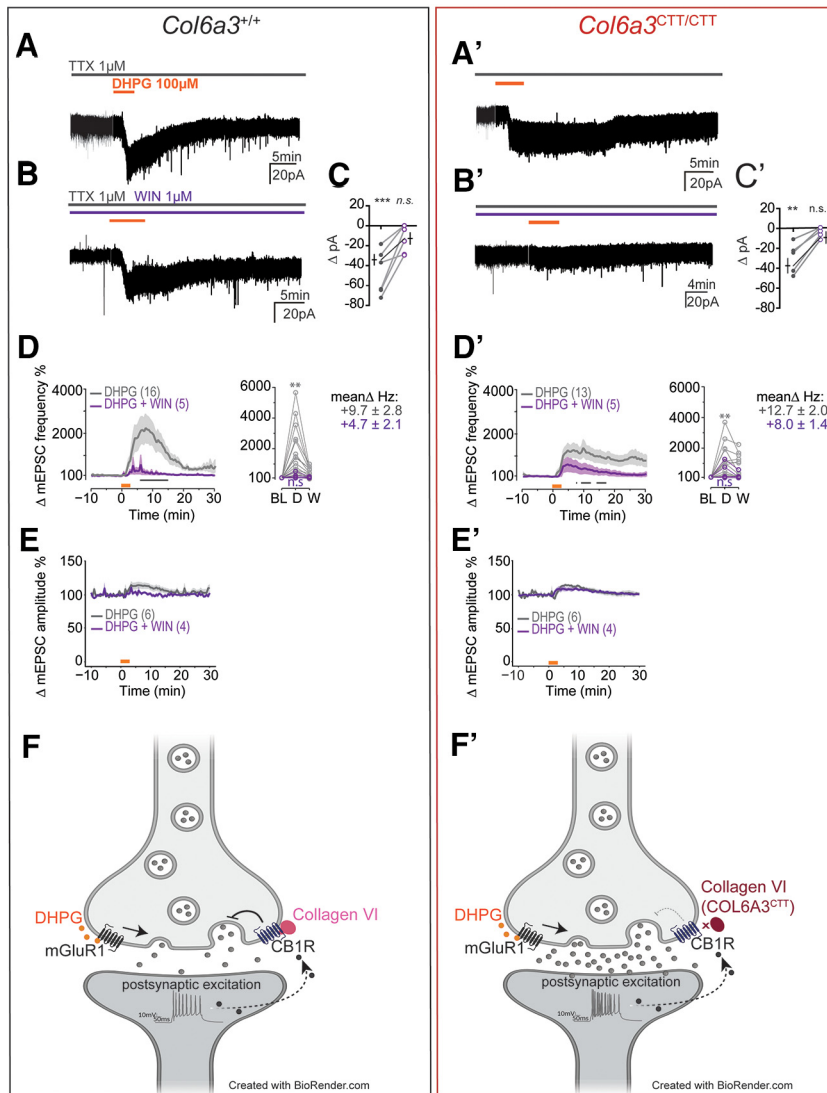
Figure 14. Impaired synaptic homeostasis of $Col6a3^{CTT/CTT}$ BPN neurons and improvement with CB1R agonist. ***A, A'***, Representative voltage-clamp response to mGluRI agonist DHPG (orange bar; 100 μM) in wild-type and $Col6a3^{CTT/CTT}$ cells, respectively, in the presence of TTX (s1 μM). ***B, B'***, Representative voltage-clamp response to DHPG in the presence of CB1R agonist WIN (purple bar; 1 μM) in wild-type and $Col6a3^{CTT/CTT}$ cells, respectively, in the presence of TTX. ***C, C'***, Quantitative summary of DHPG-evoked current in TTX alone (left) and with WIN (right) in wild-type and $Col6a3^{CTT/CTT}$ cells, respectively. Significance is with respect to baseline. ***D, D'***, Effect of DHPG on mEPSC frequency in wild-type and $Col6a3^{CTT/CTT}$ cells, respectively. DHPG causes a large increase in mEPSC frequency which then returns to baseline. This decay effect is impaired in $Col6a3^{CTT/CTT}$ mice. The effect of DHPG is blocked by WIN (purple traces), albeit more effectively in wild types. Mean and 95% confidence intervals are shown. Time points with statistically significant differences between DHPG and DHPG+WIN conditions from the same cells are indicated by black bars (RM-ANOVA, $p < 0.05$). Line plots show values at baseline (BL; 0 min), peak DHPG effect (D; 7 min), and washout (W; 25 min). ***E, E'***, Effect of DHPG on mEPSC amplitude in wild-type and $Col6a3^{CTT/CTT}$ cells, respectively. The effect of DHPG is blocked by WIN in wild types but not in $Col6a3^{CTT/CTT}$ mice. Mean and 95% confidence intervals are shown. ***F, F'***, Schematic of afferent BPN synapses in wild-type and $Col6a3^{CTT/CTT}$ mice, respectively. DHPG activates mGluRI, stimulating synaptic glutamate release. Postsynaptic neurons produce eCBs which signal retrogradely at presynaptic CB1R, suppressing glutamate release. Collagen VI facilitates CB1R function via the COL6A3 CTD. In $Col6a3^{CTT/CTT}$ mice, collagen VI modulation of CB1R is perturbed, disrupting inhibition of glutamate release and resulting in excessive glutamate release. Graphics created with BioRender.

^{CTT} genotype had a much more significant effect on the BPN proteome than that of the cerebellum (Fig. 11).

Thus, we performed *ex vivo* whole-cell patch-clamp electrophysiological recordings on BPN neurons of acute brain slices, around which collagen VI is expected to be secreted (Fig. 12A,B). The BPN consists of exclusively glutamatergic neurons (Fig. 12C), primarily conveying descending signals from the cortex to the cerebellum (Brodal and Bjaalie, 1997; Kelly and Strick, 2003;

Suzuki et al., 2012). We found that the intrinsic passive membrane properties, namely RMP, cell capacitance and input resistance (R_{in}; Extended Data Fig. 12-1), and both glutamatergic and GABAergic tone onto these cells were similar in wild-type and $Col6a3^{CTT/CTT}$ mice (Fig. 12D–M). A subset of $Col6a3^{CTT/CTT}$ neurons did have higher spontaneous EPSC (sEPSC) activity, yet as a population it did not reach statistical significance (Fig. 12I,J,L). Action potential properties were also similar between genotypes (Extended Data Fig. 12-1). In a principal component analysis of action potential and membrane properties, the cells did not segregate by genotype (Fig. 13).

The Type I metabotropic glutamate receptor (mGluR) agonist (S)$-$3,5-dihydroxyphenylglycine (DHPG) drives eCB-mediated inhibition of presynaptic inputs (Varma et al., 2001; Robbe et al., 2002; Chevaleyre and Castillo, 2003; Kushmerick et al., 2004). We therefore evaluated this response in BPN neurons of wild-type and $Col6a3^{CTT/CTT}$ mice. DHPG is known to increase membrane noise, causing traces to appear noisy (White et al., 2003; Tan et al., 2006; D'Ascenzo et al., 2009). DHPG (100 μM) applied in the presence of tetrodotoxin (TTX; 1 μM; to prevent action potential-mediated responses) caused a large significant inward current in both genotypes when compared with baseline values (WT: -36.68 ± 5.17 pA, $n = 16$, $t = 9.5$, df = 4; and $Col6a3^{CTT/CTT}$: -49.79 ± 11.22 pA, $n = 13$, $t = 5.7$, df = 4). The current evoked in $Col6a3^{CTT/CTT}$ cells failed to return to baseline values despite a prolonged washout period (>20 min), suggesting altered mGluR kinetics (Fig. 14A,A'). The current was largely and significantly attenuated by the CB1R agonist WIN (1 μM; WT:+DHPG -47.43 ± 9.03 pA, and +WIN/DHPG -12.77 ± 5.67 pA, $n = 6$, $p = 0.007$, $t = 4.4$, df = 5; and $Col6a3^{CTT/CTT}$:+DHPG -29.57 ± 6.8 pA, and +WIN/DHPG -3.66 ± 2.34 pA, $n = 5$, $p = 0.006$, $t = 5.4$, df = 4; Fig. 14B,B',C,C'), presumably via inhibition of presynaptic glutamate release. The attenuation of DHPG current by WIN was similar between genotypes (wild-type, $75.7 \pm 12.7\%$ reduction, $n = 6$; CTT/CTT, $92.5 \pm 6.0\%$ reduction, $n = 5$; Welch's t test, $p = 0.27$, $t = 1.2$, df = 7.1; Fig. 14C,C').

To assess whether the presumed action of WIN was reflected by changes in glutamate input, we measured miniature EPSC (mEPSC) activity. Unexpectedly, DHPG application potentiated glutamatergic input to BPN cells (WT: baseline 0.82 ± 0.20 Hz vs +DHPG 10.18 ± 2.95 Hz, $n = 16$, RM-ANOVA $p = 0.0003$, $F_{(2,30)} = 10.95$; $Col6a3^{CTT/CTT}$: baseline 2.01 ± 0.85 Hz vs +DHPG 14.81 ± 2.86 Hz, $n = 13$, RM-ANOVA $p = 0.0001$, $F_{(2,24)} = 13.48$; Fig. 14D,D',E,E'). The increase in mEPSC frequency caused by DHPG was similar in both genotypes: WT 10.3 ± 2.9 Hz;

$Col6a3^{CTT/CTT}$ 15.3 ± 3.3 Hz; t test $p =$ 0.27, $t = 1.1$, df = 27). This is in contrast to the previously reported rapid depression of glutamatergic input DHPG causes in accumbal and striatal cells (Robbe et al., 2002; Kreitzer and Malenka, 2007). The response was prolonged in $Col6a3^{CTT/CTT}$ cells (WT$_{wash}$: 3.03 ± 0.95 Hz; $Col6a3^{CTT/CTT}_{wash}$: 10.72 ± 2.50 Hz; % decay from $t = 7$–25 min, WT: 68 ± 7%; $Col6a3^{CTT/CTT}$: 33 ± 13%, $p < 0.03$, $t = 2.4$, df = 17.8; Fig. 14D,D'), indicating an overall exaggerated potentiation and thus an impaired adaptation to excitation.

WIN blocked this DHPG-mediated excitation in both wild-type ($n = 5$, RM-ANOVA $p = 0.07$, $F_{(2,8)} = 3.75$) and $Col6a3^{CTT/CTT}$ cells ($n = 5$, RM-ANOVA $p = 0.12$, $F_{(2,8)} = 2.8$; Fig. 14D,D'). DHPG also caused an increase in the amplitude of excitatory inputs in a proportion of cells within both genotypes (WT: baseline 11.32 ± 1.09 pA vs +DHPG 12.45 ± 0.98 pA, $n = 7$ of 15, RM-ANOVA $p = 0.02$, $F_{(2,12)} = 5.75$; and $Col6a3^{CTT/CTT}$: baseline 10.21 ± 1.27 pA vs +DHPG 11.80 ± 1.30 pA, $n = 6$ of 14, RM-ANOVA $p = 0.004$, $F_{(2,10)} = 9.76$; Fig. 14E,E'). The remaining cells did not show any statistically significant deviation of amplitude with pharmacological treatment ($p = 0.12$, $F_{(2,14)} = 2.4$, and $p = 0.07$, $F_{(2,14)} = 3.2$ for WT and $Col6a3^{CTT/CTT}$, respectively). When repeated in the presence of WIN, this increase in amplitude in some cells persisted (WT: WIN 11.99 ± 0.76 pA vs +WIN/DHPG 12.77 ± 0.70 pA, $n = 4$ of 6, RM-ANOVA $p = 0.0006$, $F_{(2,6)} = 32.3$; and $Col6a3^{CTT/CTT}$:WIN 10.55 ± 1.40 pA vs +DHPG 11.43 ± 1.52 pA, $n = 4$ of 5, RM-ANOVA $p = 0.01$, $F_{(2,6)} = 9.3$; Fig. 14E,E'). WIN did block a DHPG-induced amplitude increase in two of the four WT cells but none from the $Col6a3^{CTT/CTT}$ population. These data suggest a DHPG postsynaptic effect which may be independent of mGluRI, and which could be more prevalent in the $Col6a3^{CTT/CTT}$ cells. Taken together, these results suggest an impaired, although not completely abrogated, effect of CB1R agonism to counteract glutamatergic excitation in $Col6a3^{CTT/CTT}$ cells.

To probe the endogenous eCB tone in a small subset of cells, we treated cells with either the CB1R inverse agonist AM251 (5 μM; Fig. 15A,A', green bar) or with the CB1R agonist WIN (1 μM; Fig. 15B,B', navy bar) in TTX. AM251 preferentially evoked an outward current in WT cells ($n = 2$ of 3 cells with significant current; overall average ΔI of +4.95 ± 9.37 pA; Fig. 15C), while WIN caused mixed currents in only half the cells tested ($n = 2$ of 4 cells with significant current; overall average ΔI of −3.40 ± 10.73 pA). In contrast, AM251 evoked an outward current in only one cell from $Col6a3^{CTT/CTT}$ BPN slices (I of 11.39 pA, $n = 1$ of 4; Fig. 15C') while WIN evoked a significant outward current in two of three cells examined (overall average
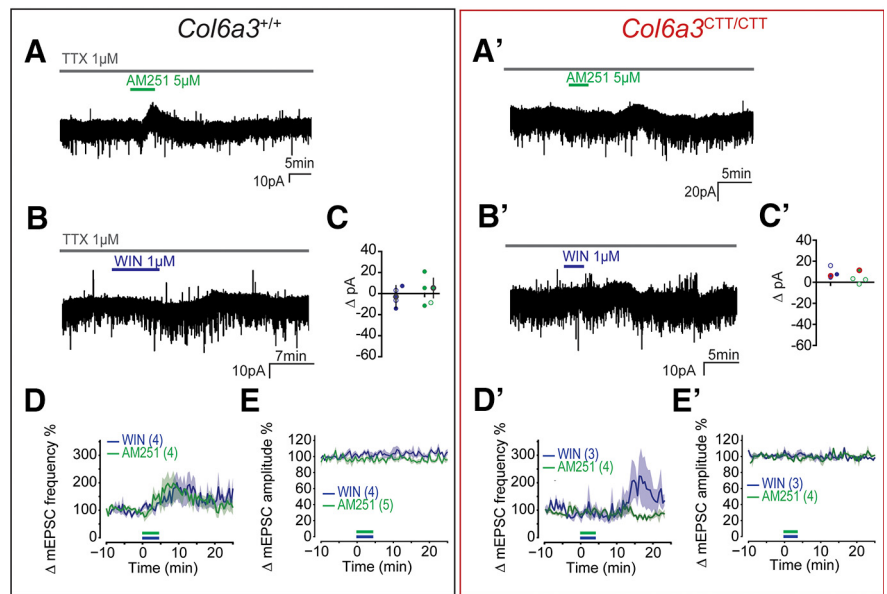
ΔI of +6.09 ± 1.56 pA). However, compared with the group baseline values in either genotype, neither compound reached statistical significance, suggesting little endogenous eCB tone on the postsynaptic membrane.

When we assessed presynaptic eCB tone in a small subset of cells, AM251 and WIN had very little effect on mEPSC frequency or amplitude in both WT and $Col6a3^{CTT/CTT}$ cells (WT frequency: baseline 3.07 ± 1.31 Hz vs +AM251 6.96 ± 2.9 Hz, $n = 4$, RM-ANOVA $p = 0.11$, $F_{(2,6)} = 3.3$; and WT: baseline 1.74 ± 0.86 Hz vs +WIN 3.29 ± 1.70 Hz, $n = 4$, RM-ANOVA $p = 0.19$, $F_{(2,6)} = 2.2$; $Col6a3^{CTT/CT}$: baseline 3.56 ± 1.49 Hz vs +AM251 4.51 ± 1.53 Hz, $n = 4$, RM-ANOVA $p = 0.35$, $F_{(2,6)} = 1.2$; and $Col6a3^{CTT/CTT}$: baseline 2.30 ± 1.32 Hz vs +WIN 1.63 ± 0.36 Hz, $n = 3$, RM-ANOVA $p = 0.38$, $F_{(2,4)} = 1.2$; Fig. 15D,E,D',E'). These data suggest there is little to no

Figure 15. Endogenous CB1R tone in BPN neurons. *A*, *A'*, Representative voltage-clamp trace to assess CB1R tone. The effect of CB1R antagonist AM251 (green bar; 5 μM) in the presence of TTX on wild-type and $Col6a3^{CTT/CTT}$ cells, respectively. *B*, *B'*, Representative voltage-clamp traces of CB1R agonist WIN (navy bar; 1 μM) in TTX on wild-type and $Col6a3^{CTT/CTT}$ cells, respectively. *C*, *C'*, Quantitative summary of AM251 and WIN currents (left, WIN; right, AM251). Circles with bold gray (wild-type)/red (CTT/CTT) border are mean ± SEM. Filled circles are statistically significant currents compared with baseline, empty circles are non-significant currents. *D*, *D'*, Effect of WIN and AM251 on mEPSC frequency in wild-type and $Col6a3^{CTT/CTT}$ cells, respectively. Mean and 95% confidence intervals are shown. *E*, *E'*, Effect of WIN and AM251 on mEPSC amplitude in wild-type and $Col6a3^{CTT/CTT}$ cells, respectively. Mean and 95% confidence intervals are shown.
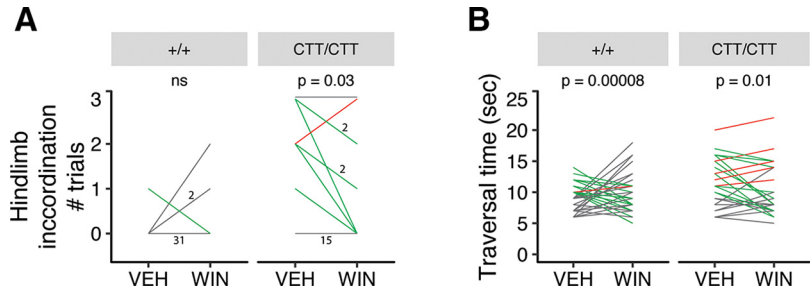

Figure 16. Cannabinoid-mediated improvement of motor control in $Col6a3^{CTT/CTT}$ mice. *A*, Effect of WIN treatment in randomized crossover design study on hindlimb incoordination on 12-mm rectangular beam. Green, performance improved by WIN; red, performance worsened with WIN; gray, baseline value of 0 (unimpaired) or performance unchanged with WIN. Number indicates number of mice with indicated trajectory. *B*, Effect of WIN treatment on traversal time of 12-mm rectangular beam. Green, performance improved by WIN; red, performance worsened with WIN; gray, baseline value below median (9.5 s) or performance unchanged with WIN. WIN was particularly beneficial for mice with poor baseline performance. Male and female mice aged 12–28 weeks, $n = 26$–34 per genotype; same mice as shown in Figure 6C,D.
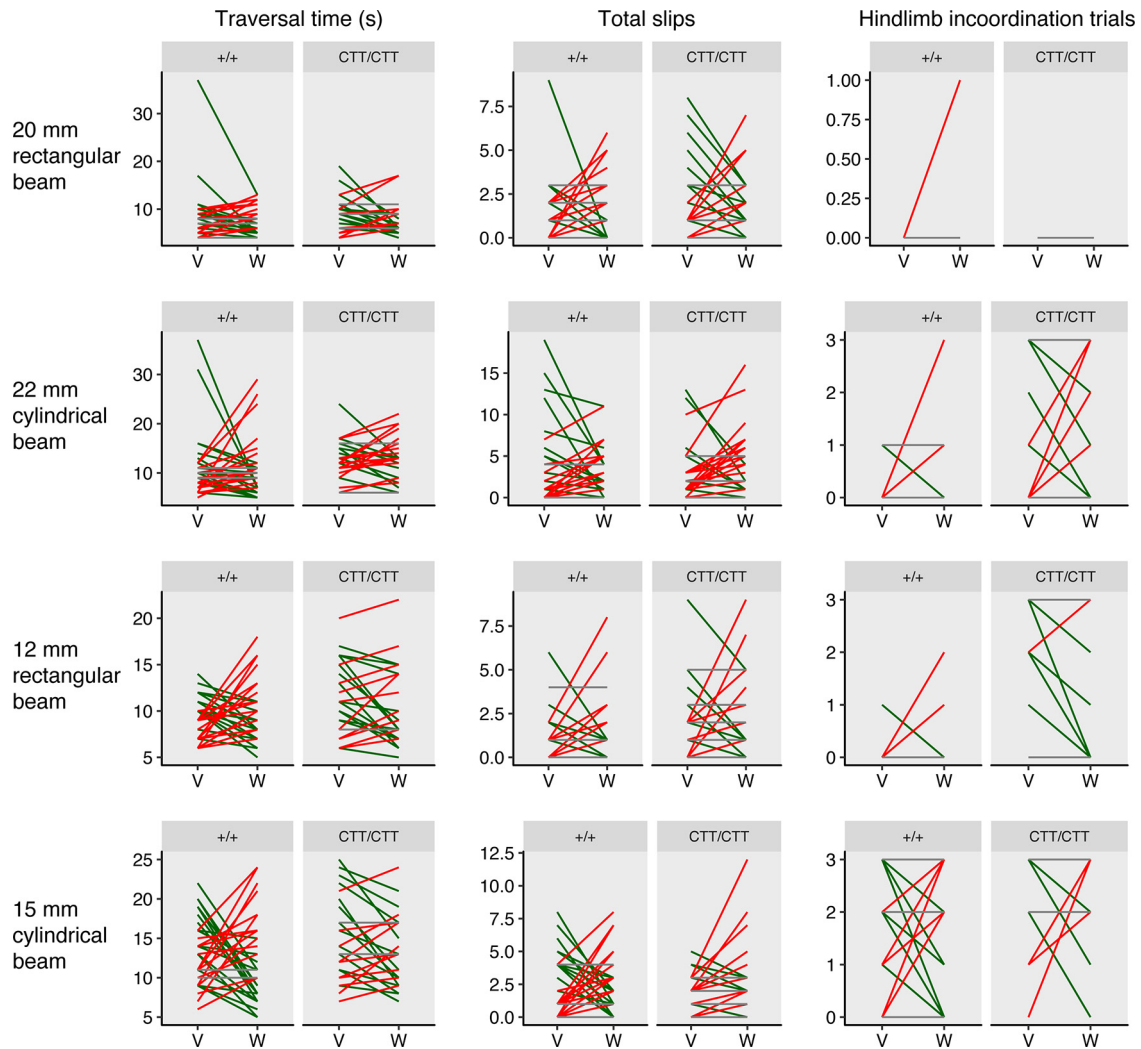
Figure 17. Full results of cannabinoid augmentation experiment. Effect of WIN (1 mg/kg, i.p.) treatment on beam walk performance. Each mouse received both WIN and vehicle in a randomized crossover design, with the two conditions separated by one to eight weeks. Testing commenced 2 h after injection. Green, performance improved by WIN; red, performance worsened with WIN; gray, performance unchanged with WIN. Male and female mice aged 12–28 weeks, n = 26–34 per genotype.

endogenous eCB tone in the BPN before DHPG stimulation. Collectively, these data demonstrate impaired synaptic homeostasis in $Col6a3^{CTT/CTT}$ neurons, possibly because of impaired CB1R function (Fig. 14F,F').

CB1R agonist rapidly improves motor performance in $Col6a3^{CTT/CTT}$ mice

We showed that BPN neurons of $Col6a3^{CTT/CTT}$ mice were impaired in their ability to restore homeostasis to excitatory input signaling, and hypothesized that this mediates at least part of their dyskinetic phenotype. We also showed that WIN could still restrain excitatory input potentiation in the BPN in $Col6a3^{CTT/CTT}$ mice, albeit with reduced efficacy. This led us to hypothesize that CB1R agonism may be an effective treatment for the dyskinesia seen in $Col6a3^{CTT/CTT}$ mice. We subjected mice to a randomized crossover study testing the effect of acute CB1R agonism on motor performance. We found that WIN treatment 2 h before the beam walk test (Morgese et al., 2007) significantly improved hindlimb coordination (Figs. 16, 17). Applying stratified analysis to evaluate the effect of WIN on values above the population median, we observed significant improvements in $Col6a3^{CTT/CTT}$ mice in hindlimb coordination

and traversal time on the 12- and 15-mm beams (paired t test: hindlimb coordination, 12-mm beam: $p = 0.03$, $t = 2.3$, df = 16; 15-mm beam: $p = 0.01$, $t = 2.7$, df = 16; traversal time, 12-mm beam: $p = 0.01$, $t = 1.5$, df = 17; 15-mm beam: $p = 0.03$, $t = 2.4$, df = 17), as well as number of slips on the 20-mm beam (paired t test, $p = 0.02$, $t = 2.9$, df = 9).

Discussion

We establish a molecular and synaptic mechanism through which the unique CTD of collagen $\alpha3$ (VI) regulates motor function, and through which variants affecting this domain engender the movement disorder dystonia. The mechanism implicates the cannabinoid receptor CB1R, which can be targeted noninvasively to improve motor performance.

$Col6a3^{CTT}$ mouse model

The $Col6a3^{CTT}$ mutation caused substantial NMD of the transcript, meaning that $Col6a3^{CTT/CTT}$ expressed a truncated COL6A3 protein at significantly lower levels than wild types. Nevertheless, the mice had a dyskinetic phenotype which was not occluded by myopathy, unlike mice with complete loss of COL6A3 function which are overtly myopathic

(Pan et al., 2013, 2014) . Like patients with variants affecting the COL6A3 CTD, the dyskinetic phenotype of *Col6a3*$^{\text{CTT}}$ mice was recessive, with heterozygous mice showing normal motor performance (Fig. 6). *Col6a3*$^{\text{CTT/CTT}}$ mice also show modestly reduced muscle strength in older mice. As reduced muscle strength is seen in unrelated mouse models of dystonia such as a cholinergic system torsinA-deficient mouse (Pappas et al., 2018), it is unclear whether it is in this case related to an effect of the CTT mutation on collagen VI function in muscle. Mitigating against this possibility is the observation that muscle histology is normal in young *Col6a3*$^{\text{CTT/CTT}}$ mice, and even aged *Col6a3*$^{\text{CTT/CTT}}$ have only a moderate myopathy (Pan et al., 2013, 2014).

The collagen-cannabinoid connection
Collagen VI is deposited in a wide range of tissues, including skeletal muscle, adipose tissue, cartilage, skin, and nervous system (Cescon et al., 2015). Interactions with a variety of extracellular matrix components and cell surface receptors have been shown, including other collagens, glycoproteins, and integrins (Cescon et al., 2015). The functional repertoire extends well beyond structural functions to include cytoprotection, regulation of myelination, macrophage recruitment, and hair growth, yet in each of these cases the mechanism, and particularly the interaction partner, remains largely unknown (Cescon et al., 2015). Here, we identify a specific receptor through which collagen VI can modulate cellular and circuit functions. CB1R has a highly plastic orthosteric binding pocket, enabling it to respond to a variety of ligands of considerably different shapes and sizes (Hua et al., 2017). Thus, collagen VI may act as a positive allosteric modulator of CB1R.

Basal pontine plasticity
The BPN links the cerebral cortex and cerebellum in an integral motor control circuit, which mediates the selection and denoising of cortical representations during motor learning (Guo et al., 2021; Wagner et al., 2019). We now show that BPN neurons are indeed capable of input potentiation, which is homeostatically counteracted by eCBs. As eCB retrograde inhibition is operative in the BPN, it may contribute to some of the key features of adaptive motor control, such as surround inhibition, which appear disrupted in dystonia. We did not find evidence for eCB-mediated synaptic depression, as is observed in the striatum and accumbens (Robbe et al., 2002; Kreitzer and Malenka, 2007). However, other paradigms for evoking synaptic depression, such as high frequency afferent stimulation, would be an interesting avenue of future investigation.

Other studies have associated collagen VI with neuroprotection. Specifically, disruption of collagen VI increased apoptosis, while exogenous collagen VI reduced stress-induced apoptosis in primary cortical/hippocampal neuronal cultures (Cheng et al., 2009; Cescon et al., 2016). We did not detect robust evidence of apoptosis in *Col6a3*$^{\text{CTT/CTT}}$ mice under basal conditions (data not shown). Further studies are required to determine whether challenging the circuit, e.g., with physiological stress, may induce apoptosis. Intriguingly, cannabinoid signaling is protective against excitotoxicity (Marsicano et al., 2003). Further studies are required to clarify whether this mechanism is at least partially responsible for the neuroprotective effect of collagen VI.

Cannabinoid modulation of motor performance
We demonstrate that cannabinoid augmentation with a CB1R agonist can improve motor outcomes in impaired *Col6a3*$^{\text{CTT/CTT}}$ mice. Although COL6A3-related dystonia is rare, our results suggest that cannabinoid augmentation may have therapeutic potential in these patients. Furthermore, this potential may generalize to other forms of dyskinesia. Indeed, several case studies and small open-label studies report a beneficial effect of cannabinoid treatment in dyskinesia (Koppel, 2015). Our mechanistic findings reported here provide a firm evidentiary basis and give fresh impetus to investigating cannabinoid-related treatment of dyskinesias.

References

Albanese A, Bhatia K, Bressman SB, Delong MR, Fahn S, Fung VSC, Hallett M, Jankovic J, Jinnah HA, Klein C, Lang AE, Mink JW, Teller JK (2013) Phenomenology and classification of dystonia: a consensus update. Mov Disord 28:863–873.

Birnboim HC, Doly J (1979) A rapid alkaline extraction procedure for screening recombinant plasmid DNA. Nucleic Acids Res 7:1513–1523.

Bonaldo P, Colombatti A (1989) The carboxyl terminus of the chicken alpha 3 chain of collagen VI is a unique mosaic structure with glycoprotein Ib-like, fibronectin type III, and Kunitz modules. J Biol Chem 264:20235–20239.

Bönnemann CG (2011) The collagen VI-related myopathies: muscle meets its matrix. Nat Rev Neurol 7:379–390.

Briñas L, Richard P, Quijano-Roy S, Gartioux C, Ledeuil C, Lacène E, Makri S, Ferreiro A, Maugenre S, Topaloglu H, Haliloglu G, Pénisson-Besnier I, Jeannet PY, Merlini L, Navarro C, Toutain A, Chaigne D, Desguerre I, de Die-Smulders C, Dunand M, et al. (2010) Early onset collagen VI myopathies: genetic and clinical correlations. Ann Neurol 68:511–520.

Brodal P, Bjaalie JG (1997) Salient anatomic features of the cortico-ponto-cerebellar pathway. Prog Brain Res 114:227–249.

Brosch M, Yu L, Hubbard T, Choudhary J (2009) Accurate and sensitive peptide identification with Mascot Percolator. J Proteome Res 8:3176–3181.

Bruderer R, Bernhardt OM, Gandhi T, Miladinović SM, Cheng LY, Messner S, Ehrenberger T, Zanotelli V, Butscheid Y, Escher C, Vitek O, Rinner O, Reiter L (2015) Extending the limits of quantitative proteome profiling with data-independent acquisition and application to acetaminophen-treated three-dimensional liver microtissues. Mol Cell Proteomics 14:1400–1410.

Calabresi P, Pisani A, Rothwell J, Ghiglieri V, Obeso JA, Picconi B (2016) Hyperkinetic disorders and loss of synaptic downscaling. Nat Neurosci 19:868–875.

Cescon M, Gattazzo F, Chen P, Bonaldo P (2015) Collagen VI at a glance. J Cell Sci 128:3525–3531.

Cescon M, Chen P, Castagnaro S, Gregorio I, Bonaldo P (2016) Lack of collagen VI promotes neurodegeneration by impairing autophagy and inducing apoptosis during aging. Aging (Albany NY) 8:1083–1098.

Cheng JS, Dubal DB, Kim DH, Legleiter J, Cheng IH, Yu GQ, Tesseur I, Wyss-Coray T, Bonaldo P, Mucke L (2009) Collagen VI protects neurons against Abeta toxicity. Nat Neurosci 12:119–121.

Chevaleyre V, Castillo PE (2003) Heterosynaptic LTD of hippocampal GABAergic synapses: a novel role of endocannabinoids in regulating excitability. Neuron 38:461–472.

Chopra RK, Ananthanarayanan VS (1982) Conformational implications of enzymatic proline hydroxylation in collagen. Proc Natl Acad Sci USA 79:7180–7184.

Concordet JP, Haeussler M (2018) CRISPOR: intuitive guide selection for CRISPR/Cas9 genome editing experiments and screens. Nucleic Acids Res 46:W242–W245.

D'Ascenzo M, Podda MV, Fellin T, Azzena GB, Haydon P, Grassi C (2009) Activation of mGluR5 induces spike afterdepolarization and enhanced excitability in medium spiny neurons of the nucleus accumbens by modulating persistent Na+ currents. J Physiol 587:3233–3250.

Demir E, Sabatelli P, Allamand V, Ferreiro A, Moghadaszadeh B, Makrelouf M, Topaloglu H, Echenne B, Merlini L, Guicheney P (2002) Mutations in COL6A3 cause severe and mild phenotypes of Ullrich congenital muscular dystrophy. Am J Hum Genet 70:1446–1458.

Dobin A, Davis CA, Schlesinger F, Drenkow J, Zaleski C, Jha S, Batut P, Chaisson M, Gingeras TR (2013) STAR: ultrafast universal RNA-seq aligner. Bioinformatics 29:15–21.

Folker ES, Baylies MK (2013) Nuclear positioning in muscle development and disease. Front Physiol 4:363.

Frik J, Merl-Pham J, Plesnila N, Mattugini N, Kjell J, Kraska J, Gómez RM, Hauck SM, Sirko S, Götz M (2018) Cross-talk between monocyte invasion and astrocyte proliferation regulates scarring in brain injury. EMBO Rep 19:e45294.

Grosche A, Hauser A, Lepper MF, Mayo R, von Toerne C, Merl-Pham J, Hauck SM (2016) The proteome of native adult Müller glial cells from murine retina. Mol Cell Proteomics 15:462–480.

Grumati P, Coletto L, Sabatelli P, Cescon M, Angelin A, Bertaggia E, Blaauw B, Urciuolo A, Tiepolo T, Merlini L, Maraldi NM, Bernardi P, Sandri M, Bonaldo P (2010) Autophagy is defective in collagen VI muscular dystrophies, and its reactivation rescues myofiber degeneration. Nat Med 16:1313–1320.

Guo JZ, Sauerbrei BA, Cohen JD, Mischiati M, Graves AR, Pisanello F, Branson KM, and Hantman AW (2021) Disrupting cortico-cerebellar communication impairs dexterity. Elife 10:e65906.

Hauck SM, Dietter J, Kramer RL, Hofmaier F, Zipplies JK, Amann B, Feuchtinger A, Deeg CA, Ueffing M (2010) Deciphering membrane-associated molecular processes in target tissue of autoimmune uveitis by label-free quantitative mass spectrometry. Mol Cell Proteomics 9:2292–2305.

Heumüller SE, Talantikite M, Napoli M, Armengaud J, Mörgelin M, Hartmann U, Sengle G, Paulsson M, Moali C, Wagener R (2019) C-terminal proteolysis of the collagen VI α3 chain by BMP-1 and proprotein convertase(s) releases endotrophin in fragments of different sizes. J Biol Chem 294:13769–13780.

Hua T, Vemuri K, Nikas SP, Laprairie RB, Wu Y, Qu L, Pu M, Korde A, Jiang S, Ho JH, Han GW, Ding K, Li X, Liu H, Hanson MA, Zhao S, Bohn LM, Makriyannis A, Stevens RC, Liu ZJ (2017) Crystal structures of agonist-bound human cannabinoid receptor CB1. Nature 547:468–471.

Irwin WA, Bergamin N, Sabatelli P, Reggiani C, Megighian A, Merlini L, Braghetta P, Columbaro M, Volpin D, Bressan GM, Bernardi P, Bonaldo P (2003) Mitochondrial dysfunction and apoptosis in myopathic mice with collagen VI deficiency. Nat Genet 35:367–371.

Kelly RM, Strick PL (2003) Cerebellar loops with motor cortex and prefrontal cortex of a nonhuman primate. J Neurosci 23:8432–8444.

Koppel BS (2015) Cannabis in the treatment of dystonia, dyskinesias, and tics. Neurother J Am Soc Exp Neurother 12:788–792.

Kreitzer AC, Malenka RC (2007) Endocannabinoid-mediated rescue of striatal LTD and motor deficits in Parkinson's disease models. Nature 445:643–647.

Kushmerick C, Price GD, Taschenberger H, Puente N, Renden R, Wadiche JI, Duvoisin RM, Grandes P, von Gersdorff H (2004) Retroinhibition of presynaptic Ca2+ currents by endocannabinoids released via postsynaptic mGluR activation at a calyx synapse. J Neurosci 24:5955–5965.

Lepper MF, Ohmayer U, von Toerne C, Maison N, Ziegler AG, Hauck SM (2018) Proteomic landscape of patient-derived CD4+ T cells in recent-onset type 1 diabetes. J Proteome Res 17:618–634.

Lo HR, Chao Y-C (2004) Rapid titer determination of baculovirus by quantitative real-time polymerase chain reaction. Biotechnol Prog 20:354–360.

Marakhonov AV, Tabakov VY, Zernov NV, Dadali EL, Sharkova IV, Skoblov MY (2018) Two novel COL6A3 mutations disrupt extracellular matrix formation and lead to myopathy from Ullrich congenital muscular dystrophy and Bethlem myopathy spectrum. Gene 672:165–171.

Marsicano G, Goodenough S, Monory K, Hermann H, Eder M, Cannich A, Azad SC, Cascio MG, Gutiérrez SO, van der Stelt M, López-Rodriguez ML, Casanova E, Schütz G, Zieglgänsberger W, Di Marzo V, Behl C, Lutz B (2003) CB1 cannabinoid receptors and on-demand defense against excitotoxicity. Science 302:84–88.

Mattugini N, Merl-Pham J, Petrozziello E, Schindler L, Bernhagen J, Hauck SM, Götz M (2018) Influence of white matter injury on gray matter reactive gliosis upon stab wound in the adult murine cerebral cortex. Glia 66:1644–1662.

Morgese MG, Cassano T, Cuomo V, Giuffrida A (2007) Anti-dyskinetic effects of cannabinoids in a rat model of Parkinson's disease: role of CB (1) and TRPV1 receptors. Exp Neurol 208:110–119.

Pan TC, Zhang RZ, Markova D, Arita M, Zhang Y, Bogdanovich S, Khurana TS, Bönnemann CG, Birk DE, Chu ML (2013) COL6A3 protein deficiency in mice leads to muscle and tendon defects similar to human collagen VI congenital muscular dystrophy. J Biol Chem 288:14320–14331.

Pan TC, Zhang RZ, Arita M, Bogdanovich S, Adams SM, Gara SK, Wagener R, Khurana TS, Birk DE, Chu ML (2014) A mouse model for dominant collagen VI disorders: heterozygous deletion of Col6a3 Exon 16. J Biol Chem 289:10293–10307.

Pappas SS, Li J, LeWitt TM, Kim JK, Monani UR, Dauer WT (2018) A cell autonomous torsinA requirement for cholinergic neuron survival and motor control. Elife 7:e36691.

Quartarone A, Pisani A (2011) Abnormal plasticity in dystonia: disruption of synaptic homeostasis. Neurobiol Dis 42:162–170.

Robbe D, Kopf M, Remaury A, Bockaert J, Manzoni OJ (2002) Endogenous cannabinoids mediate long-term synaptic depression in the nucleus accumbens. Proc Natl Acad Sci USA 99:8384–8388.

Schindelin J, Arganda-Carreras I, Frise E, Kaynig V, Longair M, Pietzsch T, Preibisch S, Rueden C, Saalfeld S, Schmid B, Tinevez J-Y, White DJ, Hartenstein V, Eliceiri K, Tomancak P, Cardona A (2012) Fiji: an open-source platform for biological-image analysis. Nat Methods 9:676–682.

Shimomura H, Lee T, Tanaka Y, Awano H, Itoh K, Nishino I, Takeshima Y (2019) Two closely spaced mutations in cis result in Ullrich congenital muscular dystrophy. Hum. Genome Var 6:1–4.

Suzuki L, Coulon P, Sabel-Goedknegt EH, Ruigrok TJH (2012) Organization of cerebral projections to identified cerebellar zones in the posterior cerebellum of the rat. J Neurosci 32:10854–10869.

Tan Y, Hori N, Carpenter DO (2006) Electrophysiological effects of three groups of glutamate metabotropic receptors in rat piriform cortex. Cell Mol Neurobiol 26:913–922.

Timpl R, Chu M (1994) Microfibrillar collagen type VI. In: Extracellular matrix assembly and structure, pp 207–242. San Diego: Academic Press.

UniProt Consortium (2019) UniProt: a worldwide hub of protein knowledge. Nucleic Acids Res 47:D506–D515.

Urciuolo A, Quarta M, Morbidoni V, Gattazzo F, Molon S, Grumati P, Montemurro F, Tedesco FS, Blaauw B, Cossu G, Vozzi G, Rando TA, Bonaldo P (2013) Collagen VI regulates satellite cell self-renewal and muscle regeneration. Nat Commun 4:1964.

Varma N, Carlson GC, Ledent C, Alger BE (2001) Metabotropic glutamate receptors drive the endocannabinoid system in hippocampus. J Neurosci 21:RC188.

Vitagliano L, Berisio R, Mazzarella L, Zagari A (2001) Structural bases of collagen stabilization induced by proline hydroxylation. Biopolymers 58:459–464.

Wagner MJ, Kim TH, Kadmon J, Nguyen ND, Ganguli S, Schnitzer MJ, Luo L (2019) Shared cortex-cerebellum dynamics in the execution and learning of a motor task. Cell 177:669–682.e24.

White AM, Kylänpää RA, Christie LA, McIntosh SJ, Irving AJ, Platt B (2003) Presynaptic group I metabotropic glutamate receptors modulate synaptic transmission in the rat superior colliculus via 4-AP sensitive K(+) channels. Br J Pharmacol 140:1421–1433.

Wilson RI, Nicoll RA (2001) Endogenous cannabinoids mediate retrograde signalling at hippocampal synapses. Nature 410:588–592.

Wiśniewski JR, Zougman A, Nagaraj N, Mann M (2009) Universal sample preparation method for proteome analysis. Nat Methods 6:359–362.

Xiao T, Baier H (2007) Lamina-specific axonal projections in the zebrafish tectum require the type IV collagen Dragnet. Nat Neurosci 10:1529–1537.

Xiao T, Staub W, Robles E, Gosse NJ, Cole GJ, Baier H (2011) Assembly of lamina-specific neuronal connections by slit bound to type IV collagen. Cell 146:164–176.

Zech M, Lam DD, Francescatto L, Schormair B, Salminen AV, Jochim A, Wieland T, Lichtner P, Peters A, Gieger C, Lochmüller H, Strom TM, Haslinger B, Katsanis N, Winkelmann J (2015) Recessive mutations in the α3 (VI) collagen gene COL6A3 cause early-onset isolated dystonia. Am J Hum Genet 96:883–893.

Zeisel A, Hochgerner H, Lönnerberg P, Johnsson A, Memic F, van der Zwan J, Häring M, Braun E, Borm LE, La Manno G, Codeluppi S, Furlan A, Lee K, Skene N, Harris KD, Hjerling-Leffler J, Arenas E, Ernfors P, Marklund U, Linnarsson S (2018) Molecular architecture of the mouse nervous system. Cell 174:999–1014.e22.

Zhang YZ, Zhao DH, Yang HP, Liu AJ, Chang XZ, Hong DJ, Bonnemann C, Yuan Y, Wu XR, Xiong H (2014) Novel collagen VI mutations identified in Chinese patients with Ullrich congenital muscular dystrophy. World J Pediatr 10:126–132.